

FLAME RETARDANT SYSTEM FOR ACRYLONITRILE-BUTADIENE-STYRENE
(ABS) POLYMER BLENDED WITH MONTMORILLONITE CLAY
VIA MELT PROCESSING

THESIS

Presented to the Graduate Council of
Southwest Texas State University
in Partial Fulfillment of the Requirements

For the Degree of
Master of Science

By

Rui Li

San Marcos, Texas
August 2002

ACKNOWLEDGEMENTS

Thanks to all the staff, and graduate and undergraduate students of the Polymer Research Group for their friendship and kindly assistance. Special thanks and deep respect to Ms. Holly Stretz, my instructor, who set a good example for me with her dauntless and creative spirit.

I would like to give my sincere appreciation and respect to Dr. Gary W. Beall, Assistant Professor of Chemistry, Director of Center for Nanophase Research, and Dr. Patrick E. Cassidy, Professor of Chemistry and Associate Vice President of Academic Affairs, both at Southwest Texas State University, for their patience and knowledgeable supervision throughout my research. I would also like to thank Dr. Stanley E. Israel, Professor of Chemistry, and Dean of the College of Science, for taking the time to review this writing.

Thanks are also extended to the Texas Institute for Material Science, University of Texas at Austin, for all the processing and mechanical testing of the polymer blends. Special thanks go to Dr. D. R. Paul's student, T. D. Fornes, H. Jijun, and P. J. Yoon (postdoctoral fellow) who assisted with operation of the instruments.

Financial support was provided by the Environmental Protection Agency. Many thanks also for the material and technical support provided by Southern Clay Products, Inc.

TABLE OF CONTENTS

ACKNOWLEDGEMENTS.....	iv
LIST OF FIGURES.....	vi
LIST OF TABLES.....	viii
ABSTRACT.....	ix
1.0 INTRODUCTION.....	1
1.1 Background.....	1
1.2 Acrylonitrile-Butadiene-Styrene (ABS) System.....	2
1.3 Montmorillonite Clay and Its Applications.....	5
2.0 EXPERIMENTAL.....	11
2.1 Materials.....	11
2.2 Blend Preparation.....	13
2.2.1 Extrusion.....	13
2.2.2 Injection Molding.....	13
2.3 Test Methods.....	15
2.3.1 Tensile.....	15
2.3.2 Notched Izod Impact.....	15
2.3.3 X-ray Diffraction.....	16
2.3.4 Flammability.....	17
3.0 RESULTS AND DISCUSSION.....	21
3.1 Composition Study of SAN/Clay Blends.....	21
3.1.1 Study of Processing Temperature.....	21
3.1.2 Tensile Test of the Blends.....	23
3.1.3 X-ray Diffraction Pattern of the Blends.....	27
3.1.4 Flammability.....	34
3.1.4.1 Flammability of SAN vs Clay Type at Low Loading.....	34
3.1.4.2 Flammability of SAN/(HE) ₂ MT vs Percentage Ash.....	36
3.2 Composition Study of ABS/Clay Blends.....	40
3.2.1 Tensile.....	40
3.2.2 Notched Izod Impact.....	44
3.2.3 X-ray Diffraction Pattern of the Blends.....	45
3.2.4 Flammability.....	47
3.3 Processing Sequence Study of ABS/Clay Blends.....	52
3.3.1 Tensile.....	53
3.3.2 Notched Izod Impact.....	55
3.3.3 X-ray Diffraction Pattern of the Blends.....	56
3.3.4 Flammability.....	57
4.0 CONCLUSION.....	59
References.....	63

LIST OF FIGURES

Figure 1.	Tortuous Pathway Model in Polymer-clay Nanocomposites.....	2
Figure 2.	Three Monomers of ABS System.....	3
Figure 3.	Transmission Electron Micrograph of Mass/Bulk ABS.....	3
Figure 4.	Transmission Electron Micrograph of Emulsion Produced ABS.....	4
Figure 5.	Structure of 2:1 Layered Silicate.....	5
Figure 6.	Illustration of Three Types of Polymer-clay Nanocomposites.....	7
Figure 7.	Chemical Structure of Quaternary Ammonium Ion.....	11
Figure 8.	Injection Mold for Fire Test.....	14
Figure 9.	Illustration of X-Ray Diffraction.....	16
Figure 10.	Oxygen Bomb Calorimeter.....	19
Figure 11.	Mass Loss Calorimeter.....	20
Figure 12.	Normalization of % Ash for SAN/(HE) ₂ MT Blends.....	22
Figure 13.	Processing Temperature Study of SAN/(HE) ₂ MT Blends Normalized to 3.8% Ash.....	23
Figure 14.	Stress/strain Diagram for SAN/(HE) ₂ MT Blends.....	24
Figure 15.	Enhancement of Young's Modulus for SAN/Clay Blends.....	25
Figure 16.	Relative Modulus Enhancement for Polymer/Clay Blends.....	26
Figure 17.	Tensile Test Results of SAN/Clay Blends.....	27
Figure 18.	X-ray Diffraction Pattern for SAN/(HE) ₂ MC Blends.....	28
Figure 19.	X-ray Diffraction Pattern for SAN/M ₂ (HT) ₂ -125 Blends.....	29
Figure 20.	X-ray Diffraction Pattern for SAN/(HE) ₂ MT Blends.....	30
Figure 21.	X-ray Diffraction Pattern for SAN/BM ₂ (HT) -125 Blends.....	31
Figure 22.	X-ray Diffraction Pattern for SAN/BM ₂ (HT) Blends.....	31
Figure 23.	Comparison of Modulus Enhancement for (HE) ₂ MT Clay Blended with SAN, S/AN/MA, and SMA-8.....	32
Figure 24.	Comparison of Tensile Strength of (HE) ₂ MT Clay Blended with SAN, S/AN/MA, and SMA-8.....	33
Figure 25.	X-ray Diffraction Pattern for SMA-8/(HE) ₂ MT Blends.....	34
Figure 26.	Plot of Heat Release Rate for SAN/Clay Blends at 35 kW/m ²	35
Figure 27.	Plot of Residual Mass for SAN/Clay Blends at 35 kW/m ²	35
Figure 28.	Plot of Heat Release Rate for SAN/(HE) ₂ MT Blends at 35 kW/m ²	37
Figure 29.	Plot of Residual Mass for SAN/(HE) ₂ MT Blends at 35 kW/m ²	37
Figure 30.	Plot of Peak Heat Release Rate for SAN/(HE) ₂ MT Blends at 35 kW/m ²	38
Figure 31.	Plot of Average Heat Release Rate at 180s for SAN/(HT) ₂ MT Blends at 35 kW/m ²	39
Figure 32.	Plot of Time to Ignition for SAN/(HE) ₂ MT Blends at 35 kW/m ²	39
Figure 33.	Comparison of Young's Modulus for ABS/Clay and SAN/Clay Blends.....	40
Figure 34.	Comparison of Modulus Enhancement for ABS/Clay and SAN/Clay Blends.....	41
Figure 35.	Stress/strain Diagram for ABS/(HE) ₂ MT Blends at 14% Rubber Content.....	42

Figure 36.	Comparison of Tensile Strength at Break Point for ABS/Clay and SAN/Clay Blends.....	43
Figure 37.	Relative Tensile Strength at Break Point for ABS/Clay and SAN/Clay Blends.....	43
Figure 38.	Elongation of ABS/Clay Blends.....	44
Figure 39.	Notched Izod Impact (J/m) for ABS/Clay Blends.....	45
Figure 40.	X-ray Diffraction Pattern for ABS/M ₂ (HT) ₂ -125.....	46
Figure 41.	X-ray Diffraction Pattern for ABS/(HE) ₂ MT.....	46
Figure 42.	Plot of Heat Release Rate for ABS/(HT) ₂ MT at 35 kW/m ²	47
Figure 43.	Plot of Residual Mass for ABS/(HT) ₂ MT Blends at 35 kW/m ²	48
Figure 44.	Plot of Peak Heat Release Rate for ABS/M ₂ (HT) ₂ -125 Blends at 35 kW/m ²	48
Figure 45.	Plot of Residual Mass Rate for ABS/ M ₂ (HT) ₂ -125 Blends.....	49
Figure 46.	Comparison of Peak Heat Release Rate for ABS/Clay Blends.....	50
Figure 47.	Comparison of Average Heat Release Rate at 180s for ABS/Clay Blends.....	50
Figure 48.	Comparison of Time to Peak for ABS/Clay Blends.....	51
Figure 49.	Comparison of Time to Ignition for ABS/Clay Blends.....	51
Figure 50.	Comparison of Residual Mass for ABS/Clay Blends.....	52
Figure 51.	Young's Modulus for Simultaneous vs Masterbatch ABS/Clay.....	53
Figure 52.	Tensile Strength for Simultaneous vs Masterbatch ABS/Clay Blends.....	54
Figure 53.	Stress/strain Diagram for ABS/(HE) ₂ MT Blends at 22.5% Rubber Content.....	54
Figure 54.	Elongation for Simultaneous vs Masterbatch ABS/Clay Blends.....	55
Figure 55.	Impact Test Results for Simultaneous vs Masterbatch ABS/Clay Blends.....	56
Figure 56.	X-ray Diffraction Pattern for Simultaneous vs Masterbatch ABS/Clay Blends.....	57
Figure 57.	Comparison of Heat Release Rate at 35 kW/m ² for Simultaneous vs Masterbatch ABS/SAN/Clay Blends.....	58
Figure 58.	Comparison of Residual Mass at 35 kW/m ² for Simultaneous vs Masterbatch ABS/SAN/Clay Blends.....	58

LIST OF TABLES

Table 1.	Original Cone Calorimeter Data for Polymer/Clay Blends.....	10
Table 2.	Physical Properties of Montmorillonite Clay.....	12
Table 3.	Physical Properties of Polymer Materials.....	12
Table 4.	Parameters for Molding on Tensile/Izod Bars.....	14
Table 5.	Parameters for Molding on Fire-test Plaques.....	14
Table 6.	Original D-space vs Blended D-spacing for MMT Clay/SAN Blends.....	28
Table 7.	Polymers used in the study of the effect of MA vs AN.....	32
Table 8.	Summary of Heat Release Rate Data at 35 kW/m ² for SAN/Clay Blends.....	36

ABSTRACT

This research focused on modification of acrylonitrile-butadiene-styrene (ABS) polymer with montmorillonite (MMT) clay, a non-halogenated additive, to enhance fire retardancy. ABS is a primary component of plastic computer housings, and formulation of a non-halogenated fire retardant in ABS would allow the original equipment manufacturers (OEMs) to recycle the plastic housing in compliance with a pending European ban on halogenated additives in computers. This study investigated potential trade-offs between mechanical properties vs fire retardancy of ABS/clay blends. Further, to understand the morphology of the clay in these blends, we blended five clays with a model polymer matrix, styrene-acrylonitrile (SAN). We varied the surface modification of the clay (quaternary ammonium ions) in order to achieve compatibility and therefore dispersion of the inorganic filler in the melt.

(HE)₂MT and/or M₂(HT)₂-125-modified clay (bishydroxyethyl and dimethyl dihydrogenated tallow quaternary ammonium ions respectively) showed improvement of fire retardancy to an ABS system, lowering the peak heat release rate (PHRR). This reduction in PHRR was a nonlinear function of clay loading. The addition of MMT clay to SAN matrix and/or ABS system showed an increase in tensile modulus, as well as decrease in tensile strength. Impact strength dropped significantly in an ABS system with the loading of the clay. A small variation in rubber content ($\pm 5\%$) with the same clay content did not affect fire retardant behavior significantly, but partially restored impact resistance.

1.0 INTRODUCTION

1.1 Background

Currently some 18.7 million computer housings are disposed of per year in landfills.¹ Life expectancy of the current computers is decreasing due to the higher turn over rate in the computer industry. ABS, a primary component of plastic computer housings is traditionally fire retarded by brominated biphenyls.² A major concern of the original equipment manufacturer is that a brominated fire retardant system will prevent the recycling of disposed computer housings, since any halogenated recycle content is boycotted in the European market. The European literature has blamed brominated fire retardants for the production of dioxins when incinerated, and even for human fetal development problems *via* exposure at the office.³ Therefore, an alternative recyclable fire retardant will be of commercial interest.

Recent studies in nanocomposites demonstrate that incorporation of montmorillonite (MMT) clays into polymer systems such as nylon, polystyrene (PS), and polypropylene (PP) can enhance the fire retardancy by lowering the peak heat release rate (PHRR) of the system.⁴ The stacking of impermeable clay layers theoretically mandate a tortuous pathway through the nanocomposite char (Figure 1), which improves the flame retardancy of the blends by limiting the rate of release of flammable combustion off-gases.⁵ Gilman has shown recently that for polymer nanocomposites, the clay appears to enhance the formation of the char during combustion; and the char may act as an

insulator and mass transport barrier, slowing the escape of the volatile gases produced by polymer degradation.⁶ Furthermore, clay platelets are more durable during reprocessing than long fibers and are thus inherently more recyclable.

This research focuses on the modification of styrene-acrylonitrile (SAN) and ABS blends with montmorillonite clay to enhance fire retardance with considerable attention to the potential trade-off of mechanical properties in ABS system. Five clays with various surface treatments were blended into various ABS systems.

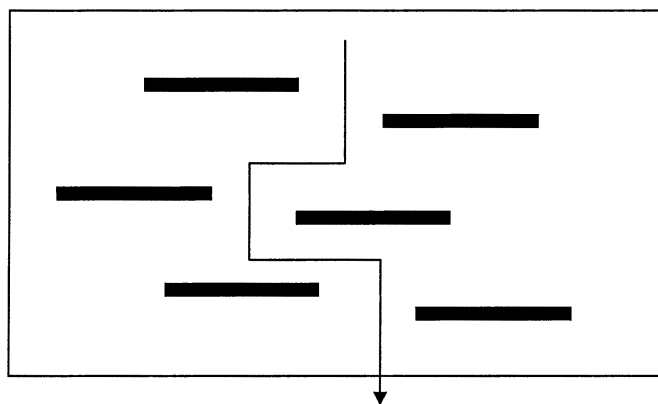


Figure 1. Tortuous Pathway Model in Polymer-clay Nanocomposites

1.2 Acrylonitrile/Butadiene/Styrene System

Acrylonitrile-butadiene-styrene (ABS) polymers are composed of an elastomer (B) dispersed as a particulate phase in a thermoplastic matrix of styrene-acrylonitrile copolymer (SAN). The presence of SAN grafted onto the elastomeric phase, usually polybutadiene or butadiene copolymer, compatibilizes the rubber with the plastic SAN phase.⁷ The monomers for ABS system are depicted in Figure 2.

Polybutadiene has carbon-carbon double bonds remaining after polymerization, which are active sites available for grafting. During final polymerization, two phases, polymers

of butadiene and styrene-acrylonitrile, are formed, which are compatibilized by grafting at their interface.

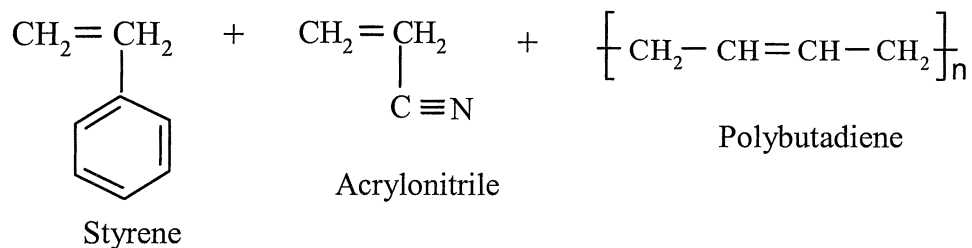


Figure 2. Three Monomers of ABS System

There are two main process for producing commercial ABS.⁸ Mass or bulk ABS (M-ABS) is made by polymerizing styrene and acrylonitrile monomers in the presence of a dissolved butadiene-based rubber to which some grafting occurs. As the styrene-acrylonitrile (SAN) copolymer is formed, phase separation occurs followed by phase inversion, which results in relatively large rubber particles having SAN occlusions. The rubber phase is a kind of cellular (salami) structure (Figure 3).

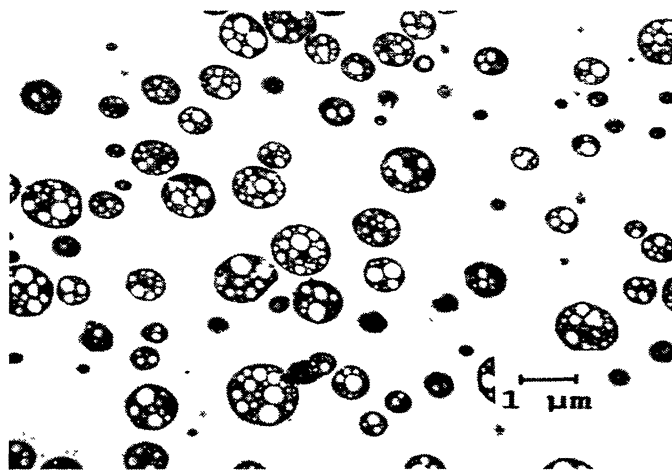


Figure 3. Transmission Electron Micrograph of Mass/Bulk ABS⁹

The second process, emulsion produced ABS (E-ABS), is made by a two-step polymerization. First butadiene is polymerized to form a rubber; often it is a butadiene-based copolymer. Next styrene and acrylonitrile are polymerized in the presence of the butadiene-based rubber particles to produce the SAN-grafted rubber and the SAN matrix. E-ABS contains a very small amount of SAN occluded in the PB domain, and usually is a kind of core-shell structure (Figure 4).

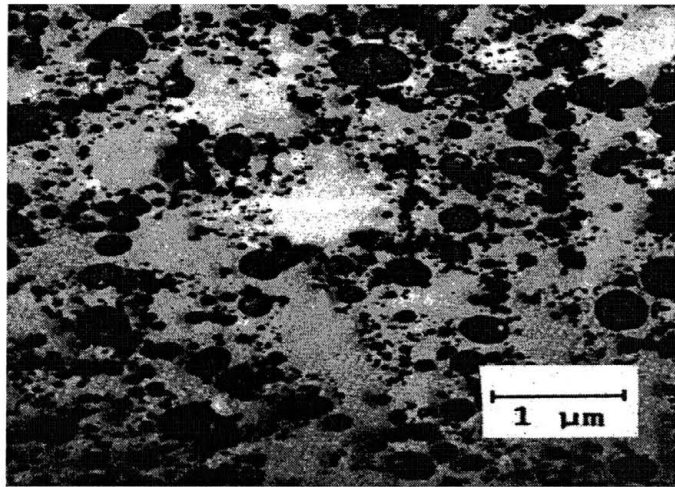


Figure 4. Transmission Electron Micrograph of Emulsion Produced ABS⁹

The mechanical properties of ABS are controlled by the compositional variables of its three phases: the SAN matrix, the polybutadiene rubber particles, and the grafted SAN at the interface between the matrix and the rubber particles. Toughness is a primary consideration in the selection of ABS systems for many applications, and morphology of the butadiene phase in the system is designed to dissipate impact energy. The inherent ductility of the system depends on the composition of the SAN copolymer. ABS has broad application as an engineering plastic, for example as an impact modifier in blends such as ABS/PC, since blend properties can be varied by the controlling the ratio of ABS to PC. Global manufacturers, such as IBM, likely show an increasing interest in ABS

blends for computer housings due to the processing costs involved in adding PC, especially if the fire retardancy issue could be resolved for ABS.¹⁰

1.3 Montmorillonite Clay and Its Applications

The montmorillonite clay used in this research is originally extracted from bentonite rock. Most commonly, Bentonite rock is formed by sedimentation of volcanic ash and subsequent “diagenesis” to clay. “Diagenesis” can be defined as the set of processes, including solution, that alter sediments at low temperatures after they are formed in nature. Another less common origin is the hydrothermal alteration of volcanic rocks

Montmorillonite clays have layered lattice structures in which two fused-silica tetrahedral sheets sandwich an edge-shared octahedral sheet of either aluminium or

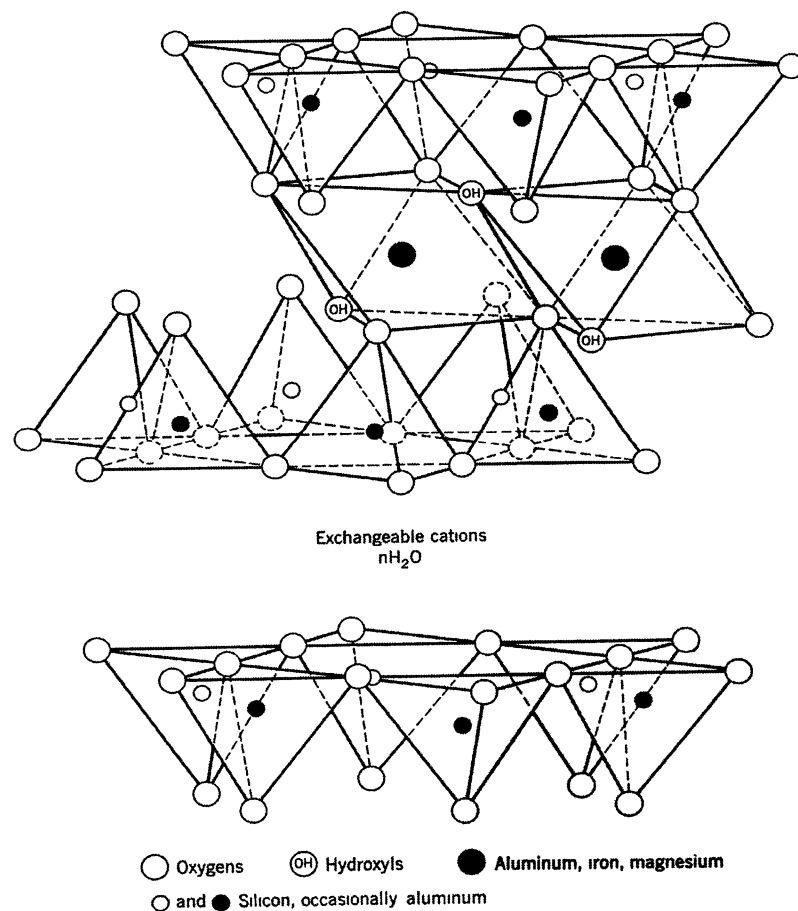


Figure 5. Structure of 2:1 Layered Silicate¹¹

magnesium (Figure 5). The layer thickness is around 1 nm and the lateral dimensions of these layers may vary from 200 Å to several microns. Stacking of the layers leads to regular van der Waals gaps called interlayers or galleries. The distance between the repeat platelets is termed the d-spacing or basal spacing, and is usually calculated from X-ray diffraction patterns (XRD). These clays are “turbostratic” which is a kind of structure with two-dimensional long-range order, but without the third dimensional order, and, therefore, each clay plate bears no crystal graphic relation in the ab plane to any other plate.

Isomorphous substitution of Al^{3+} for Si^{4+} in the tetrahedral lattice and of Mg^{2+} for Al^{3+} in the octahedral sheet causes an excess of negative charge on the platelet, which is counterbalanced in nature by cations such as Ca^{2+} and Na^+ situated between the layers. In order to make these hydrophilic MMT clays more organophilic, the hydrated cations of the interlayer can be exchanged with surfactants such as alkylammonium ions, alkylphosphonium ions and other organic cations.

The term “nanocomposite” usually describes a two-phase material where one of the phases is dispersed on a nanometer level. Polymer-clay nanocomposites were first reported in the literature as early as the 1960s, when Blumstein demonstrated polymerization of vinyl monomers incorporated into montmorillonite clay.¹² It was first demonstrated by the Toyota group in 1990 that nylon 6-clay nanocomposites can be developed using alkylammonium surfactants to compatibilize the surface chemistry of the hydrophilic clay and hydrophobic polymer matrix.¹³

There are three general approaches developed by several groups to prepare polymer-clay nanocomposites.

- In-situ: Monomer (solvent) is blended with the clay, followed by polymerization.¹³⁻¹⁵
- Solution: Polymer is dissolved in a solvent and then blended with the clay, followed by evaporation of solvent.¹⁶
- Melt processing: Dispersing clay in a polymer melt using extrusion or other melt blending equipment.¹⁷⁻¹⁸

The dispersion of clay particles in a polymer matrix can result in the formation of three types of nanocomposite particles (Figure 6). They are phase-separated, intercalated and delaminated (or exfoliated).^{15,17} When the polymer is unable to incorporate between the silicate sheets, a phase-separated composite is obtained. The clay tactoids are simply dispersed as a segregated phase resulting in conventional inorganic-filled polymer blend. These tactoids will result in an X-ray pattern with no spacing change compared to the original d-spacing of the clay.

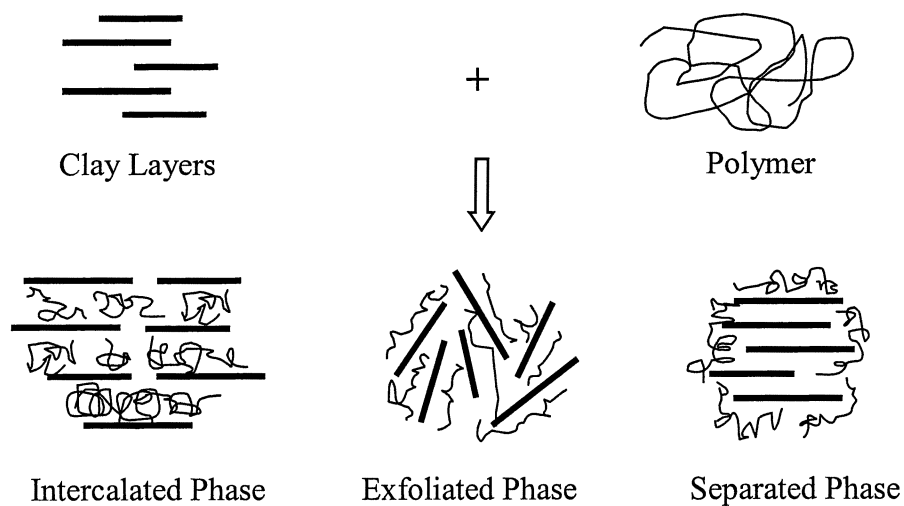


Figure 6. Illustration of Three Types of Polymer-clay Nanocomposites

An intercalated structure has been formed, when one or more extended polymer chains is regularly inserted between the gallery, resulting in well-ordered, alternating polymeric and inorganic layers. Intercalation of polymer chain will give an X-ray pattern with a d-spacing larger than that of the original clay.

The delaminated (or exfoliated) structures represent the extreme case of clay structure disruption and result when the individual silicate layers are no longer clustered. With a delaminated structure, basal X-ray diffraction peaks will not be observed because of a large spacing between the layers (the case of oriented exfoliated structure) or because the platelets are randomly dispersed. Transmission electronic microscopy (TEM) is used to further characterize the nanocomposite morphology, since both the intercalated and exfoliated phases can coexist in the polymer matrix.

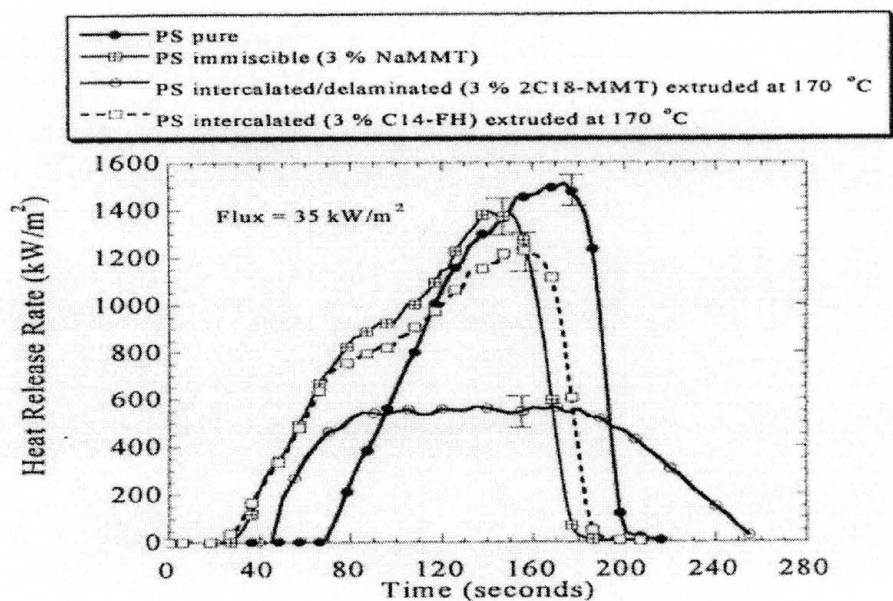
Much current research is focused on polymer-clay nanocomposites arising from their unique properties. For example, the Toyota research group demonstrated that the mechanical properties of nylon 6/clay nanocomposites, at a loading of only 4.2 wt% clay, show substantial improvement over those for the pure nylon-6. The modulus doubled, the tensile strength increased more than 50%, and the heat distortion temperature increased by 80 °C compared to the pure polymer.¹⁴ All of these improvements were seen without loss of impact resistance.

The first mention of the potential flame retardant properties of polymer-clay nanocomposites appears in a 1976 Japanese patent on nylon-6 MMT nanocomposites.¹⁹ The Toyota group reported that nylon 6/clay blends also improve the flame retardant properties in 1993.¹⁴ However, not until more recent studies of improved thermal stability were reported by Giannelis and his coworkers in both a

polydimethylsiloxane(PDMS)/clay nanocomposite and in a polyimide/clay nanocomposite did serious evaluation of the flammability properties of these materials begin.^{20, 21} The melt processing method has been studied by the Giannelis group. They showed that a phase-separated polyimide/clay mixture, which contained the same amount of silicate (10 wt.%) as the intercalated and delaminated nanocomposite, showed no enhancement in the thermal stability. This reveals that the nano-level dispersion is critical to improve thermal stability.

Recent work done by Gilman and his coworkers, using cone calorimetry, has quantitatively characterized the reduced flammability of a number of other polymer-layered silicate nanocomposites.^{22, 23} The cone calorimeter data are shown in Table 1. First, Gilman found that separated PS/clay blends did not show enhanced fire retardant properties. Second, the study found that either intercalated or exfoliated blends with low clay loading (2% to 5%) showed improvement for fire retardancy. Third, a hybrid intercalated/exfoliated state coexisting in the polymer-clay blend also showed enhanced fire retardancy. One unresolved and critical issue is which state, intercalated or separated state, will improve fire retardant properties most.

Further, it is unclear how clays will disperse in ABS systems using melt processing, both with respect to clay micro-structure and with respect to the overall micro-structure of the multi-phase ABS systems. Previous studies have shown that the clay has the potential to fire retard polymeric system. This research will focus on whether clay can fire retard an ABS system through melt processing and how clay will influence the mechanical properties of ABS.



Dispersion State of Sample	Residue Yield (%) ± 0.5	Peak Heat Release Rate (kW/m ²) (%)	Mean Heat Release Rate (kW/m ²) (%)
Neat Nylon-6	1	1010	603
Nylon-6 with 5% silicate exfoliated	6	378, (63%)	304, (50%)
Neat Polystyrene (PS)	0	1120	703
PS with 3% silicate immiscible	3	1080	715
PS with 3% silicate intercalated/exfoliated	4	567, (48%)	444, (38%)
Neat Polypropylene	0	1525	536
PP with 2% silicated intercalated	5	450, (70%)	322, (40%)

Table 1. Original Cone Calorimeter Data for Polymer/Clay Blends²³

2.0 EXPERIMENTAL

2.1 Materials

All montmorillonite clays were supplied by Southern Clay Products (SCP) in a white powder form, and were used as received. The chemical formulas of quaternary ammonium salts used in this research are depicted in Figure 7.

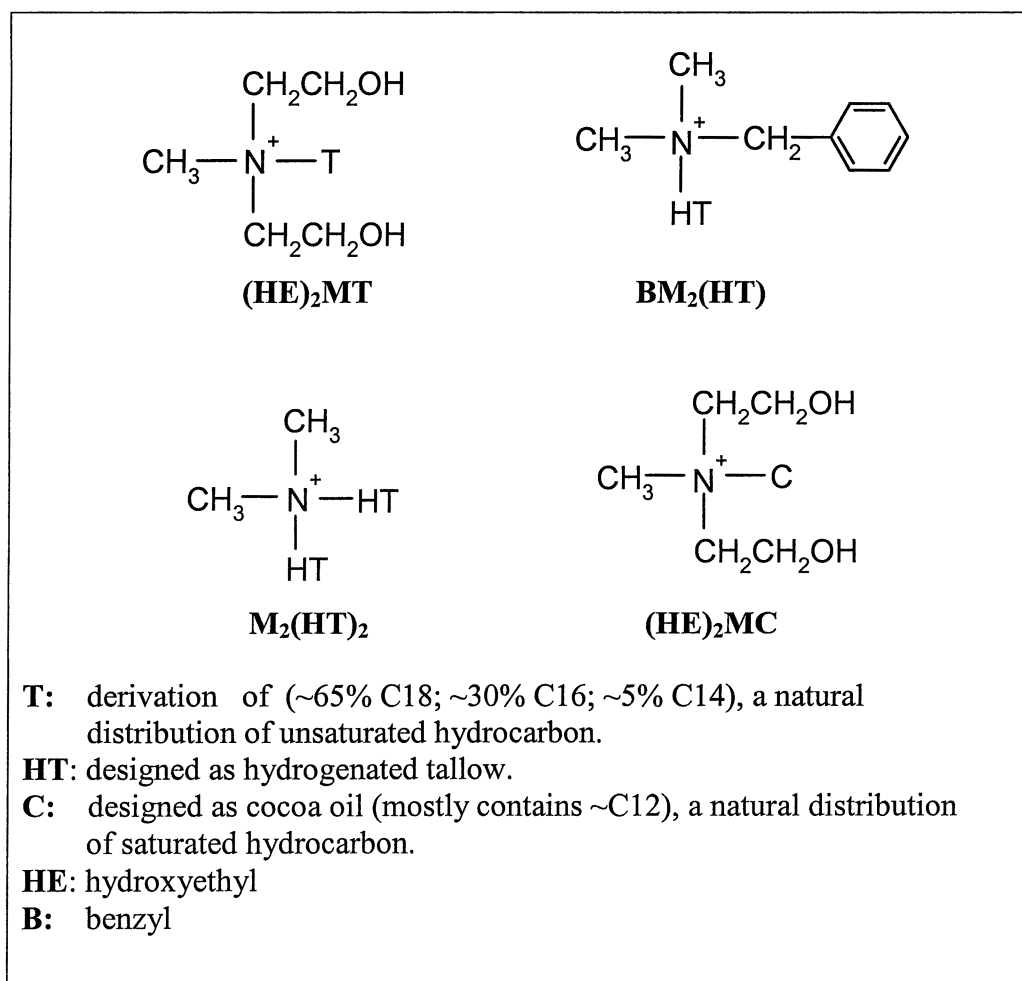


Figure 7. Chemical Structure of Quaternary Ammonium Ion

The technical data provided by SCP for five clays modified with quaternary ammonium at different exchange ratio used in this study are summarized in Table 2. All polymers used in this Study are commercial products summarized in Table 3.

Table 2. Physical Properties of Montmorillonite Clay

MMT Clay	Commercial Brand	Modifier Concentration (meq/100g)	Weight Loss on Ignition (%)	d-spacing (Å)
M ₂ (HT) ₂ -125	15A	125	43	31.5
(HE) ₂ MT	30B	90	30	18.5
BM ₂ (HT)-125	10A	125	39	19.2
(HE) ₂ MC		95	25.5	14.5
BM ₂ (HT)		95	32.1	18.5
Exchange capacity of the Cloisite clay used is normally 95 meq/100g resin (MER). Over-exchanged clays are designed "-125"; clays exchanged to capacity have no notation.				

Table 3. Physical Properties of Polymer Materials

Material	Company	Comment
Cycolac 5500 ABS	GE Plastics	
Rubber-grafted g-SAN	Chiele Industries Inc (Korea)	Mw=90,000g/mol * ¹ Graft ratio=0.52% Rubber(%)=45%
Tyrl 100 SAN	Dow Chemical Company	Mw=152,000g/mol * ² AN(%)=25%
* ¹ : provided by manufacturer. * ² : Paul, D. R., "Synthesis and characterization of an amine-functional SAN for the compatibilization of PC/ABS blends," Polymer, 40 (1999) 3069-3082		

2.2 Blend Preparation

2.2.1 Extrusion

All the blends were prepared by melt mixing in a Haake co-rotating, intermeshing twin-screw extruder with a length-to-diameter ratio (L/D) of 30, located in polymer processing lab at University of Texas at Austin. Prior to melt blending and injection molding, all materials were dried in a vacuum oven overnight at 80 °C. An extrusion temperature of 220 °C and screw speed of 280 rpm were held constant. In order to accurately compare the active inorganic structural MMT quantities, MMT levels are reported as an ash percentage. Ashing was performed at 900 °C for at least 1 hour.

2.2.2 Injection Molding

Prior to molding, all blends were dried again overnight in a vacuum oven. Injection molding for tensile and Izod bars (ASTMD636 type I and ASTM D256 respectively) as well as for fire test plaques was performed on a Allrounder 305-210-700 injection molding machine. Fire test specimens were prepared using a mold specially designed for this study, 0.32 cm thick and 10 cm x 10 cm in area, and side-gated so as to provide orientation of the clay particles along an axis perpendicular to the escaping volatile gases and flame (Figure 8).

All molding parameters were held constant. Blends were injected at a barrel temperature of 260 °C and mold temperature of 150 °C. Mold parameters were set as shown in Table 4 for tensile/Izod bars and Table 5 for fire-test plaques, respectively.

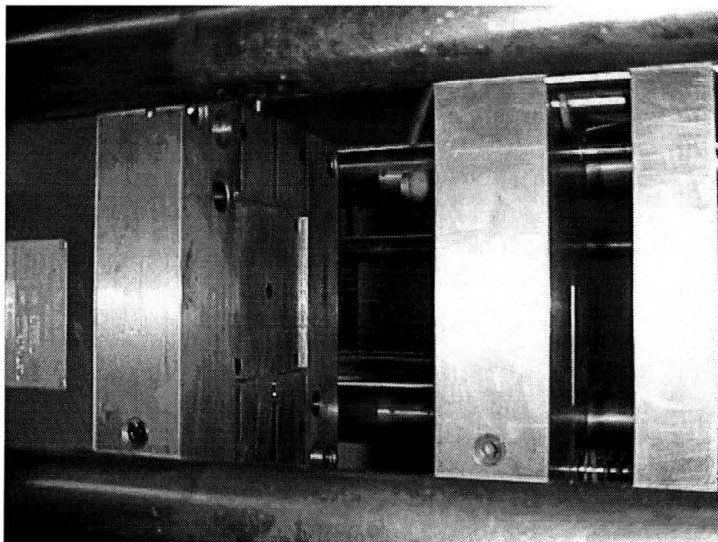


Figure 8. Injection Mold for Fire Test

Table 4. Parameters for Molding on Tensile/Izod Bars

Delayed injection	10 sec.	Dosage	17
Injection time	43 sec.	Injection speed	14.1
Holding pressure	60 sec.	Injection retract stop	14.4
Cooling time	200 sec.	Holding pressure	11.8
Die open time	10 sec.		

Table 5. Parameters for Molding on Fire-test Plaques

Delayed injection	10 sec.	Dosage	30.5
Injection time	130 sec.	Injection speed	20
Holding pressure	70 sec.	Injection retract stop	30
Cooling time	260 sec.	Holding pressure	10.6
Die open time	10 sec.		

2.3 Test Methods

2.3.1 Tensile

Among the many mechanical properties of plastic materials, tensile properties are probably the most frequently considered, evaluated, and used throughout the industry. Modulus and tensile strength properties were tested on a Sintech model ID tensile machine with a computerized data acquisition system. Five to ten dogbone-shaped, injection-molded specimens were tested. Tensile modulus values were measured using a 25 mm extensometer and a crosshead speed of 0.5 cm/min. All tensile strength measurements were made at the same crosshead speed as the tensile modulus values. Average values of at least five specimens were taken for Young's modulus and tensile stress. Standard deviations for all data are below $\pm 10\%$.

Through all the tensile experiments, samples of SAN blends show brittle behavior, while samples of ABS blends show ductile behavior. For brittle samples (SAN blends), the maximum stress achieved just prior to the sample breaking was taken as the tensile stress for these brittle blends. For ductile samples (ABS blends), the stress measured at the first maximum point at which the specimen yields (necking starts), was taken as the tensile stress for these ductile blends.

2.3.2 Notched Izod Impact

The Notched Izod test measures a material's resistance to impact from a swinging pendulum. Izod impact is defined as the kinetic energy needed to initiate fracture and continue the fracture until the specimen is broken. This test can be used as a quick and easy quality check to determine if a material meets specific impact properties or to compare materials for general toughness. The specimen is clamped with the notched side

facing the striking edge of the pendulum, and pendulum is released and allowed to strike through the specimen.

The test result is typically the average of 6 specimens, measured at room temperature. Standard deviations for these data are below $\pm 10\%$ of the mean. The standard specimen for ASTM D256 is 64 x 12.7 x 3.2 mm ($2\frac{1}{2}$ x $\frac{1}{2}$ x $\frac{1}{8}$ inch). The most common specimen thickness is 3.2 mm (0.125 inch). ASTM impact energy is expressed in J/m. The higher the resulting number, the tougher the material.

2.3.3 X-ray Diffraction

Figure 9 shows the idealized Bragg X-ray diffraction in two dimensions between two consecutive clay layers (two scattering planes) that are separated by a specific d-spacing. X-rays of wavelength λ are intercepted at the incident angle θ . D-spacing can be calculated by using Bragg' law:

$$\sin \theta = n\lambda / 2d$$

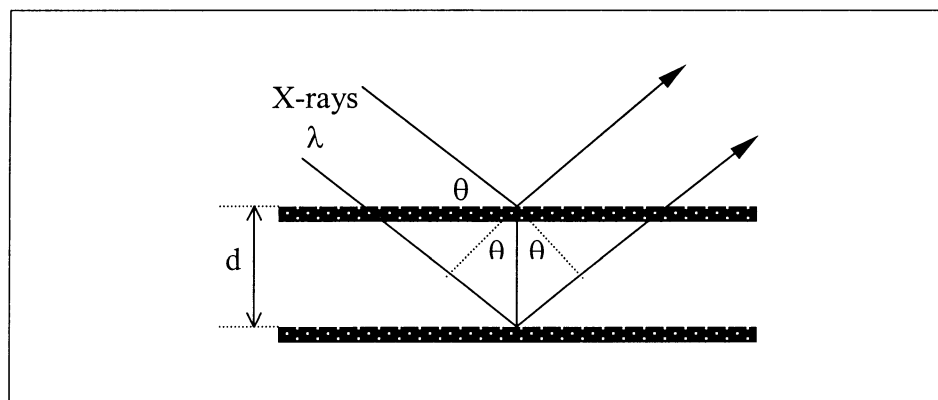


Figure 9. Illustration of X-Ray Diffraction

The intercalation of the polymer chains usually increases the interlayer spacing, in comparison with the original d-spacing of the clay used, which leads to a shift of the diffraction peak towards lower angle values. For exfoliated nanocomposites, diffraction peaks are not observed, due to the random and homogeneous dispersion of clay layers in the polymer matrix. Wide-angle X-ray (Sintag XDS 2000) in the reflectance mode was used in this study, and provided by Southern Clay Products.

2.3.4 Flammability

The potential fire hazard of any material depends on many factors, generally including ignitability, heat release rate, peak heat release rate, mass loss rate, smoke evolution, and toxicity of the smoke. We concentrated on measuring three key factors, produced when the specimen is burning with an open flame. First, heat release rate (HRR) is defined as the flux of heat produced per unit of time (kW/m^2). HRR, in particular peak HRR (PHRR), which contributed to fire spread speed of flame in actual fire scenarios, is the most important parameter to evaluate fire safety.²⁴ Second, ignitability is determined by measuring time from initial exposure to time of sustained flaming (with the assistance of the spark igniter every four seconds). Third, mass loss rate is defined as the percentage of mass lost per unit time. Higher percentage of mass remaining may prevent the collapse of objects while humans are escaping, and serve as insulators to slow the spread of the fire. The data collected from our lab are:

- Peak heat release rate (PHRR)
- Average heat release rate (AHRR) at 180s
- Time to peak (TTP)

- Time to Ignition (TTI)
- Mass remaining (%)

The heat of combustion is the quantity of heat released when unit quantity of a fuel is fully oxidized. These are determined using an oxygen bomb calorimeter and are well reported in handbooks (Figure 10).²⁵ If all fires involved complete oxidation, the amount of released heat could be determined simply by weighing the sample as it burns and multiplying the mass loss by the heat of combustion. In reality, oxidation of organics to pure CO₂ and H₂O is never complete but an effective heat of combustion can be measured for a given material when burned at a given heat flux under constant ventilation conditions. Heat release could then be determined as a product of the effective heat of combustion and the mass loss rate. Realistically the combustion process cannot be modeled so simply. Mass loss is determined by a balance mechanism, and net heat flux through the cone is determined from a thermopile arranged just above the heaters. Both outputs together are considered in evaluating the fire behavior.

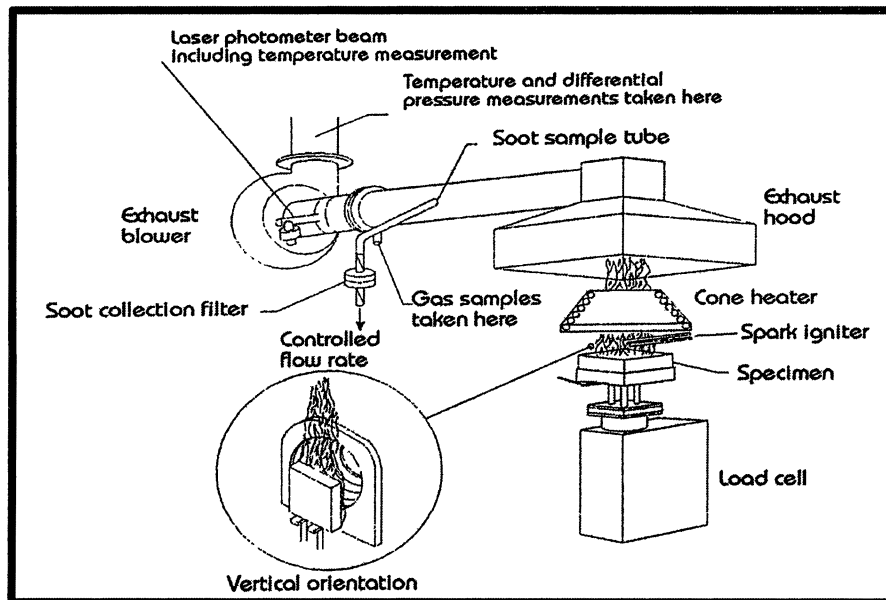


Figure 10. Oxygen Bomb Calorimeter²⁵

Our data are calculated from differences in voltages of the thermopiles connected at the entrance and exit of the mass loss calorimeter. HRR values reported here are taken however, from thermopile measurements, since effective heats of combustion during nonisothermal burning are difficult to obtain. These voltages are converted to heat measurements by a periodic methane calibration.

Figure 11 shows the mass loss calorimeter (MLC) manufactured by Fire Testing Technology Ltd. All the specimens were square (10cm × 10cm); and wrapped in aluminum foil with an edge frame on top of the sample. The standard procedure used involves exposing specimens to an external radiant heat flux in a horizontal orientation. The heat flux was set at 35 kW/m², which is approximately that used in UL-94, an industry standard method for rating materials for electronic parts such as computer housings.

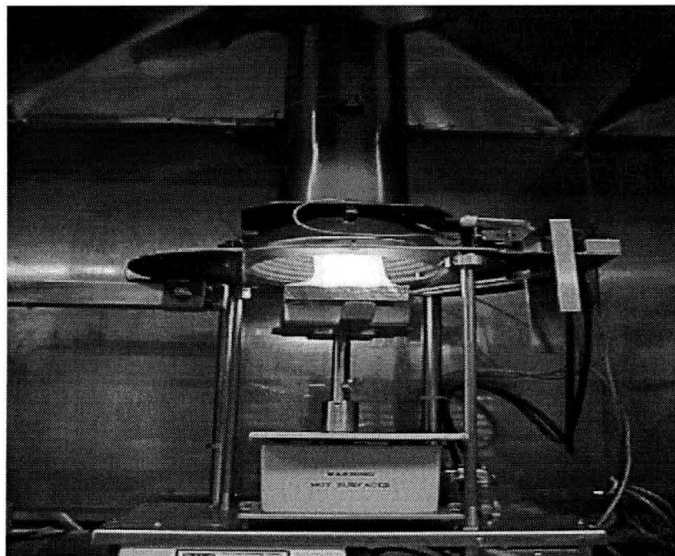


Figure 11. Mass Loss Calorimeter

Tests were generally conducted for 15 minutes (900s). Under exposure to the radiant heat flux, off-gas from each specimen was ignited by a high-voltage spark igniter every 4 seconds. HRR was plotted as a function of time. Of particular interest is the PHRR, which is a characteristic indicator of the overall heat release properties of the material.²⁵ In addition, continuous remaining mass percentage was plotted against time (seconds). The data were compiled using an EXCEL program modified for this purpose by H. A. Stretz.

3.0 RESULTS AND DISCUSSION

3.1 Composition Study of SAN/Clay Blends

Styrene-acrylonitrile copolymer (SAN) is the matrix for a two- or three-phase commercial ABS system. If the polymer itself is already present as three phases, and the clay is a fourth phase, the complexity of structure/property relationships is too great to understand behavior, at least initially. Therefore, using SAN/clay blends provides a simpler model for structure/property interactions than the more complex, but commercially interesting ABS/clay blends. It should be noted that the viscosity and ductility of the SAN is much different than that of the multiphase ABS; but the clay will probably end up residing in the SAN matrix, because the butadiene phase is cross-linked. Therefore, the resulting mechanical and flammability properties of SAN/clay blends can lend insight into the more complex ABS/clay system.

3.1.1 Study of Processing Temperature

A cursory survey of processing temperature *vs* exfoliation was performed using SAN and (HE)₂MT clay at 3.8% ash (approximately). At this experiment, ash percentage varied slightly around 3.8% ash for the SAN/(HE)₂MT blends due to the variations in packing of the feed during the extrusion processing. Therefore, original data illustrated in Figure 12 were mathematically normalized to 3.8% ash. We assume a linear relationship between modulus and % ash in this range of clay loading, while the real relationship between modulus and % ash could be either a linear or a non-linear function on each different case.

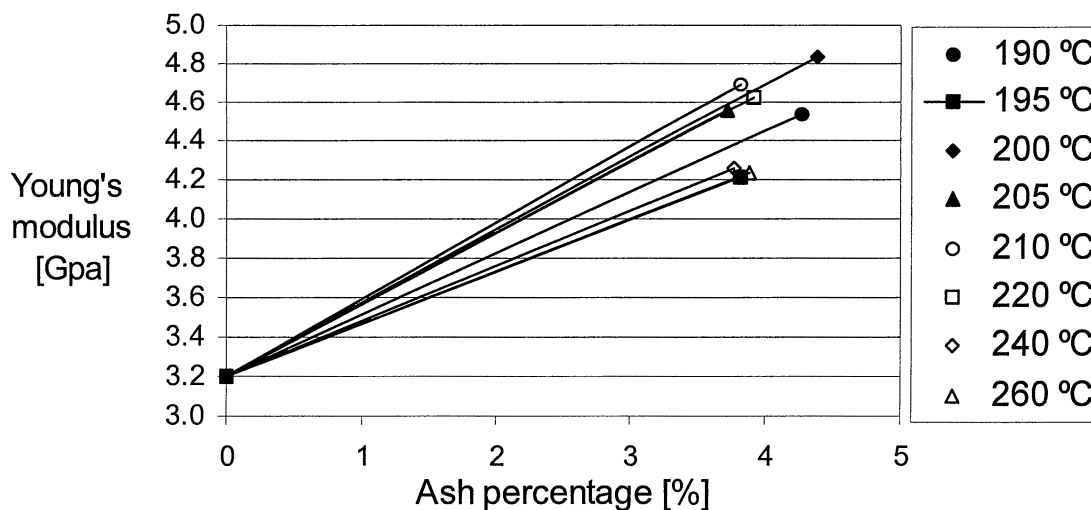
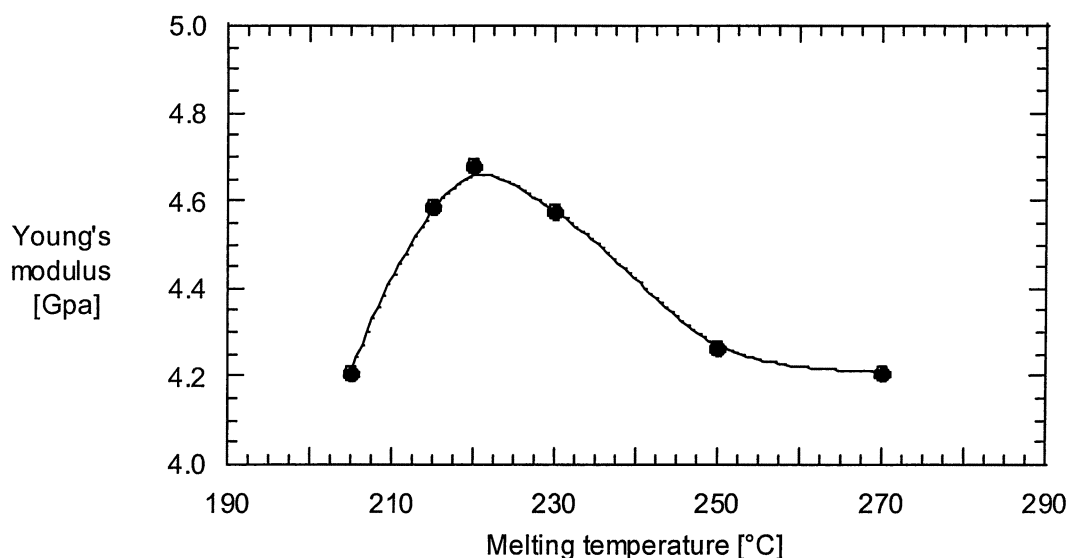


Figure 12. Normalization of % Ash for SAN/(HE)₂MT Blends

Previous work done by Dr. Paul's group demonstrated that exfoliation was measured by the highest modulus obtained for nylon-6/clay nanocomposites.²⁶ Exfoliation can be commonly measured by XRD, but SAN/clay blends in this study showed complex patterns in the XRD, therefore, modulus was determined to be the best overall indicator of level of exfoliation. However, modulus cannot indicate the absolute value of the exfoliation; it indicates only the relative exfoliation degree to some extent. Figure 13 shows the Young's modulus for SAN/(HE)₂MT blends at different melt temperatures after the clay ash percentage has been normalized to 3.8% ash. The optimum modulus was obtained at a melting temperature of 220 °C.



**Figure 13. Processing Temperature Study of SAN/(HE)₂MT Blends
Normalized to 3.8% Ash**

3.1.2 Tensile Test of the Blends

Mechanical tests were performed on SAN/clay blends by varying the clay loading at 0, 5, 8.5 and 12.5 wt% clay in the feed. Results are reported *vs* % ash for two reasons. First, the accurate composition of the surface-treated clay required by industry can be mathematically calculated by ash percentage. Second, the interaction of the polymer with a high modulus material (ie: the aluminosilicate has a modulus estimated to be over 50 times that of the polymer) is a significant contribution to the modulus enhancement of these nanocomposite blends. Organic clay content varies with the identity and exchange ratio of the quaternary ammonium ion, but can be back-calculated from the reported ash values using “% organic” shown in section 2.1.

Figure 14 shows the original stress/strain diagram obtained from tensile tests. The specimens did not yield during tensile tests, which was not surprising since unmodified SAN is itself relatively brittle.

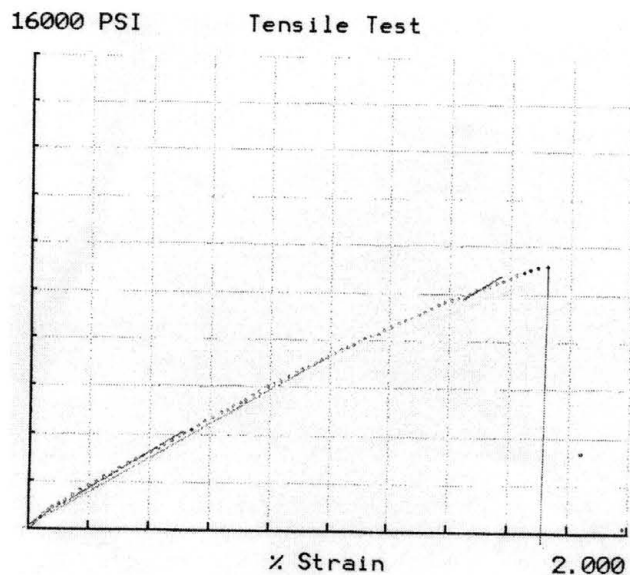


Figure 14 Stress/strain Diagram for SAN/(HE)₂MT Blends

Figure 15 shows that (HE)₂MT clay provides the highest enhancement of Young's modulus, almost doubling with addition of modified 7.5 % clay. All four other types of MMT clay have separately increased modulus by at least 50% over the bulk polymer with the addition of about 7.5 ash% loading. (HE)₂MC, M₂(HT)₂-125 and BM₂(HT)-125 clays in SAN show an initially increasing slope, which then plateaued. The plateau effect in the Figure 15, which is seen for many polymer/clay nano-blends, could be explained by several theories. The cause for this behavior probably cannot be attributed to only one theory. The first theory is the "percolation effect". As the concentration of individual platelets increases in the melt, they crowd each other and cannot "tumble" into random orientations. Thus the platelets exhibit more orientation. This effect would reduce modulus along axes transverse and perpendicular to the direction of flow.²⁷ The second theory possibly contributing to the plateau in modulus is the crowding at high clay levels, or packing. Clay may be in the aggregate form as clay concentration increases because the room available to swell and randomly disperse becomes less. The contribution of a

platelet in aggregate form to modulus enhancement is much less than the contribution of a dispersed platelet due to decreased surface area available. Another possible reason is molecular degradation. For instance, degradation in molecular weight increases as % clay (and therefore % impurity) in the polymer increases. Molecular weight degradations have been measured in polycarbonate nanocomposites and shown to be significant contributions to the plateau effect, since at some critical molecular weight, entanglement density becomes low enough that modulus is affected.²⁸

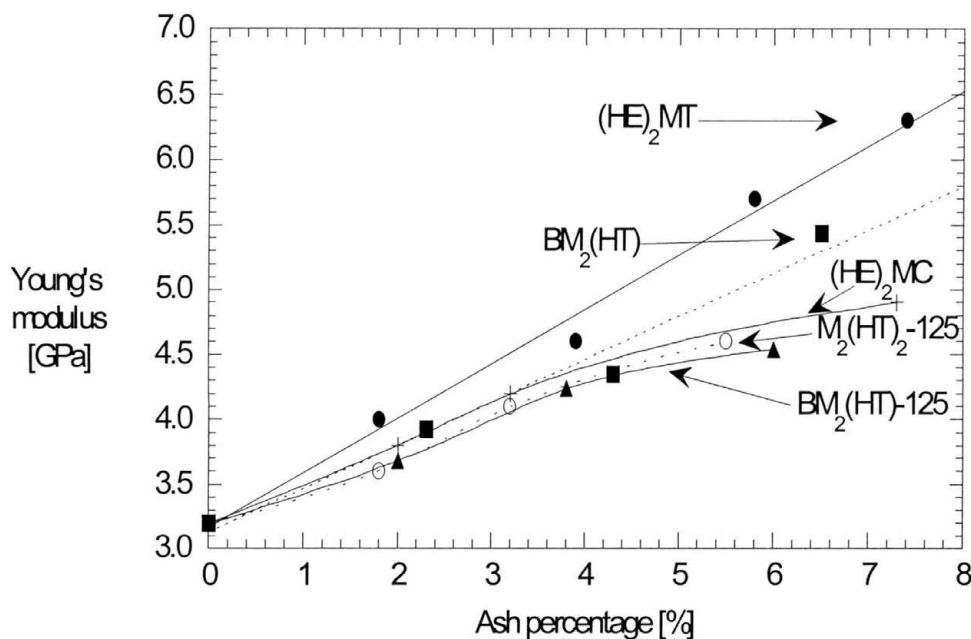


Figure 15. Enhancement of Young's Modulus for SAN/Clay Blends

Figure 16 shows the relative modulus enhancement for SAN/clay blends compared to analogous blends with nylon, polycarbonate and poly(butylene terephthalate). The clay in SAN with maximum modulus enhancement is still less effective than optimized clay/polymer blends for nylon and PC clay/polymer blends for nylon and PC.

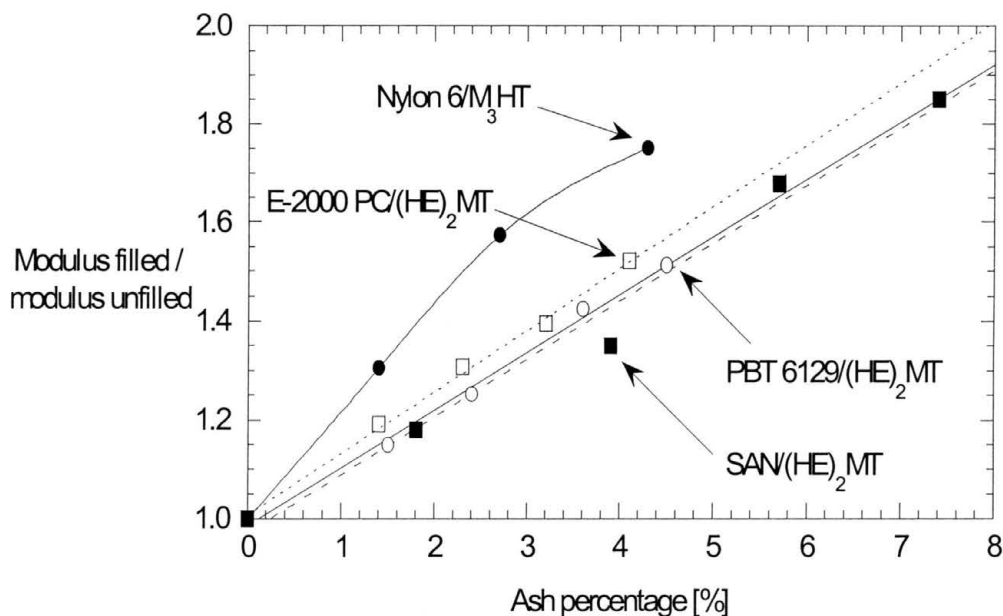


Figure 16. Relative Modulus Enhancement for Polymer/Clay Blends

The stress-at-break expresses the ultimate strength that the material bears before fracture. All of these SAN nanocomposites broke in a brittle manner as expected, since SAN is brittle. The tensile stress of the blends is plotted vs the silicate ash content in Figure 17, which shows that tensile stress of SAN/clay blends decreased with an increasing amount of the clay for all blends. The SAN may be sensitive to large tactoids (stress concentration) at the break point. No correlation between tensile strength and tensile modulus has been found for these five SAN/clay blends. Noticeably, tensile strength of nylon-6/clay and/or PC/clay nanocomposites increased with an increasing amount of the clay, since nylon and PC are ductile materials. The decrease in tensile strength could be viewed as correlated to loss of impact strength.

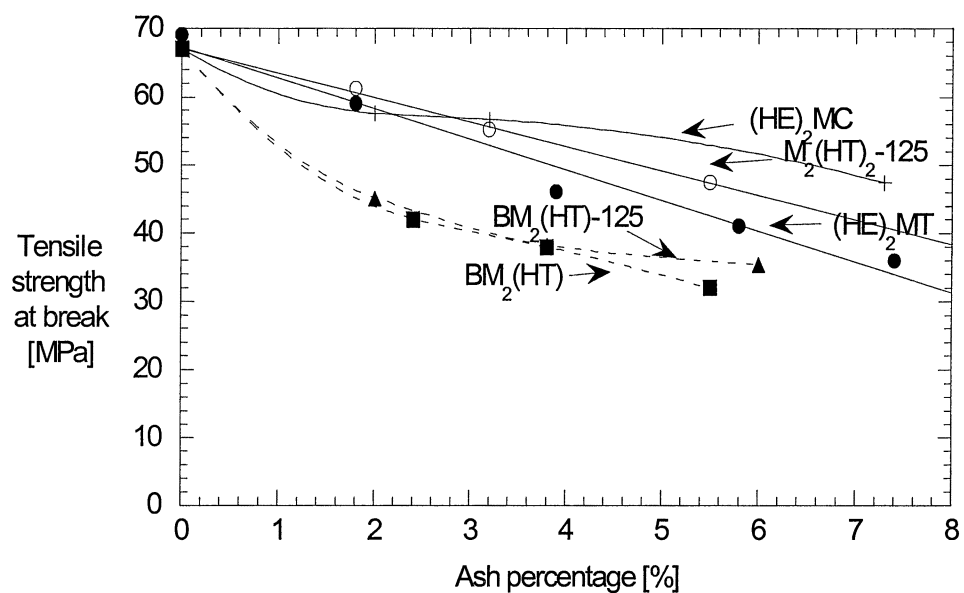


Figure 17. Tensile Test Results of SAN/Clay Blends

3.1.3 X-ray Diffraction Pattern of the Blends

X-ray diffraction patterns were determined for all samples, which identified both d-spacing changes in the clays during intercalation and extent of disappearance of the peaks during exfoliation (Table 6). Furthermore, there are two morphologies or phases of the clay, which can be identified in our X-ray diffractions:

- **first**, a state where the clay tactoids are unaltered from their original d-spacing.
- **second**, a state where the clay tactoids are mainly intercalated with some exfoliated state.

MMT Clay	d-spacing (Å) in original clay	d-spacing after processing in SAN/Clay Blends (Å)	change in d-spacing (Å)
M ₂ (HT) ₂ -125	31.5	31.9	0.4
(HE) ₂ MT	18.5	32.5	14.0
BM ₂ (HT)-125	19.2	30.2	11.0
(HE) ₂ MC	14.5	14.2	-0.3
BM ₂ (HT)	18.5	34.5	16.0

Table 6. Original D-space vs Blended D-spacing for MMT Clay/SAN Blends

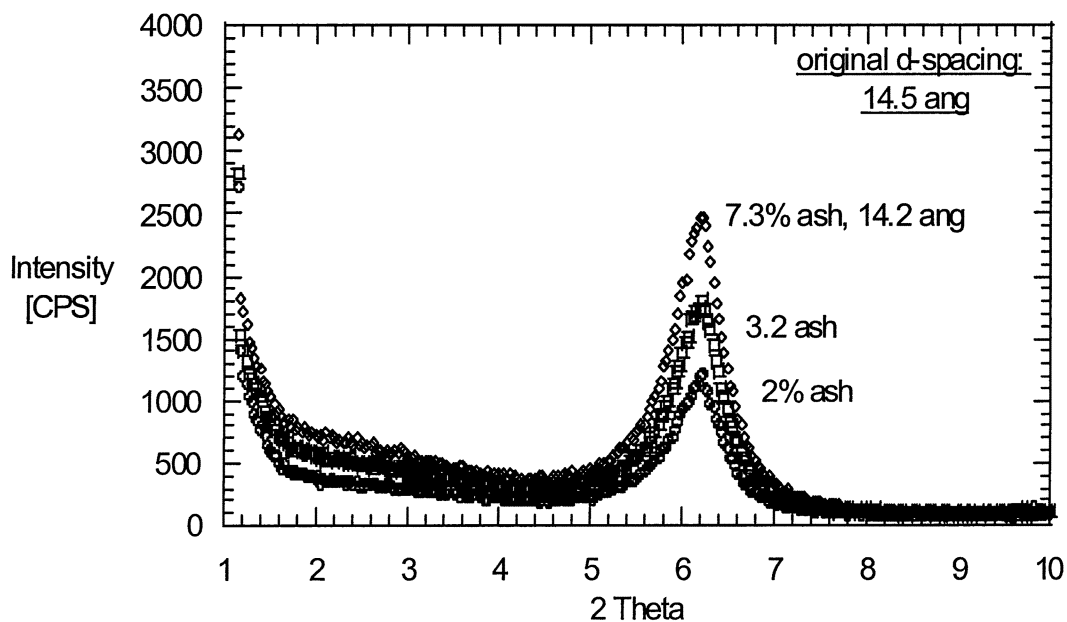


Figure 18. X-ray Diffraction Pattern for SAN/(HE)₂MC Blends

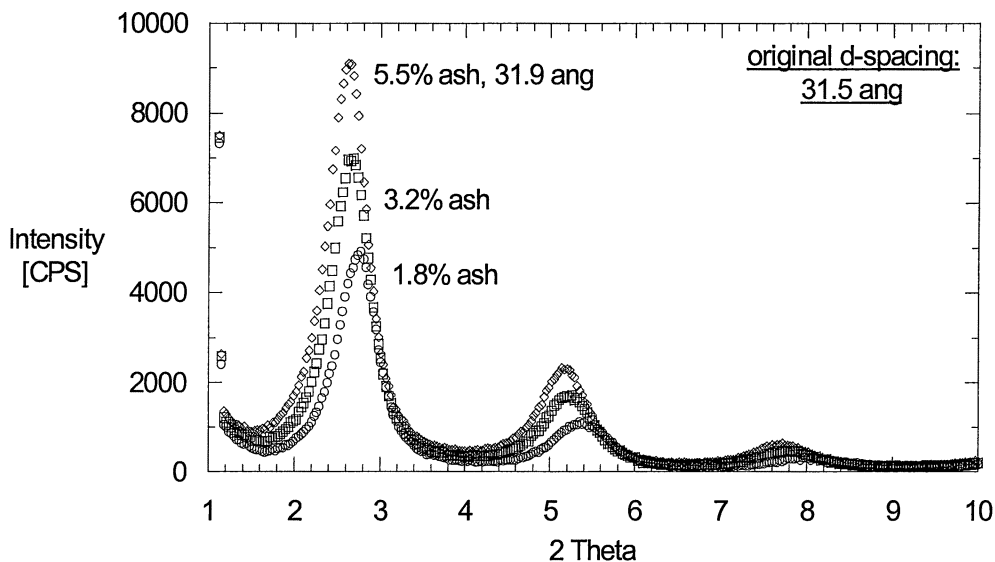


Figure 19. X-ray Diffraction Pattern for SAN/M₂(HT)₂-125 Blends

Figure 18 and 19 show the first type of morphology. The d-spacing changes are -0.3 Å for SAN/(HE)₂MC blends and $+0.4$ Å for SAN/M₂(HT)₂-125 blends, respectively, compared to the original d-spacing of each clay. Such a small d-spacing change (0.3 or 0.4 Å) could be the experimental deviation; therefore, we concluded that no polymer intercalated into the clay layers for these two SAN/clay blends, since non-expanded d-spacings were detected at the X-ray diffraction.

Figure 20, 21 and 22 show the second type of morphology observed for SAN/(HE)₂MT, SAN/BM₂(HT)-125 and SAN/BM₂(HT) blends, respectively. The d-spacings of these blends all increased and the diffraction peak of these blends all shifted toward lower angle values. Additionally, a drift baseline was exhibited in these three XRD, indicating some extent of exfoliation. The second type of morphology is then a

hybrid, mainly intercalated phase, mixed with some exfoliated platelets. We also found that SAN/(HE)₂MT blends exhibit the highest modulus with the highest baseline compared to the other four clays. No correlation trends have been found between the height of the intercalated peaks and the modulus enhancement.

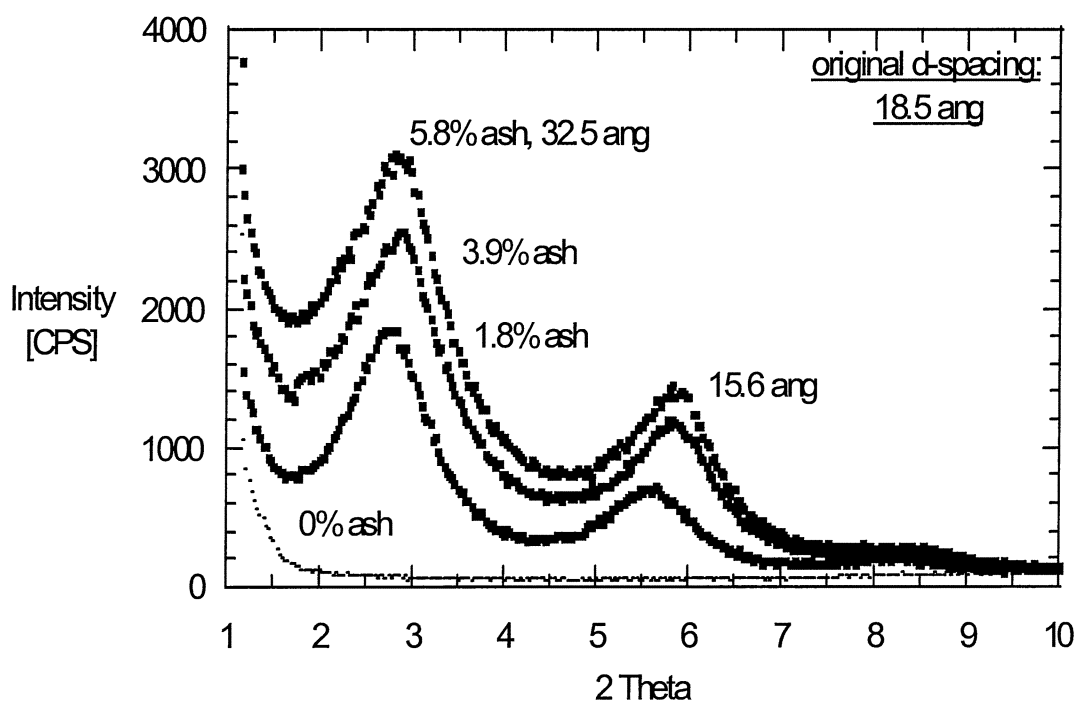


Figure 20. X-ray Diffraction Pattern for SAN/(HE)₂MT Blends

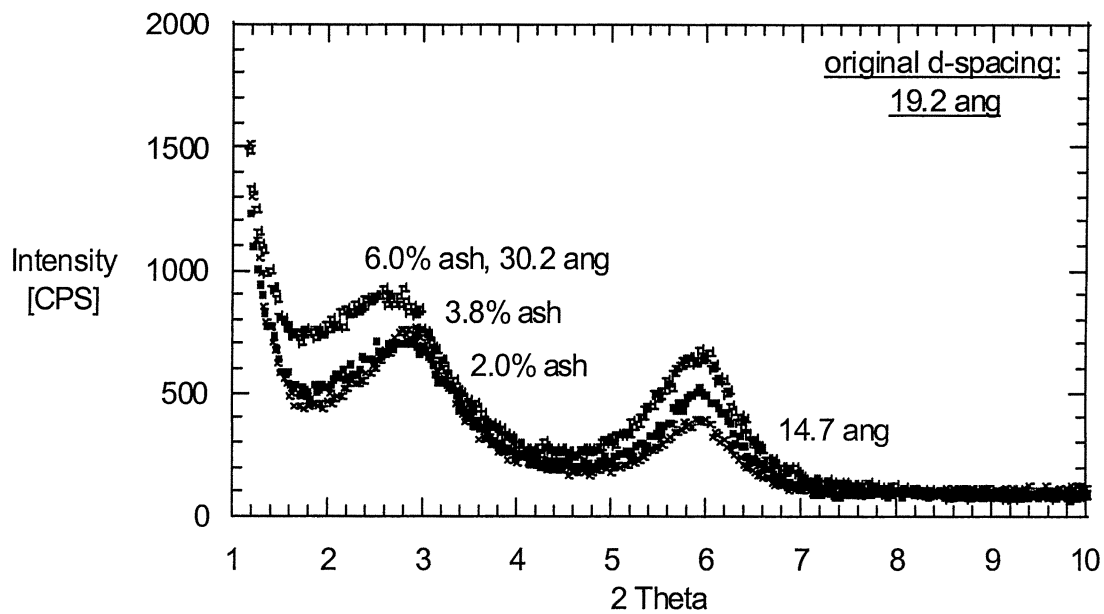


Figure 21. X-ray Diffraction Pattern for SAN/BM₂(HT) -125 Blends

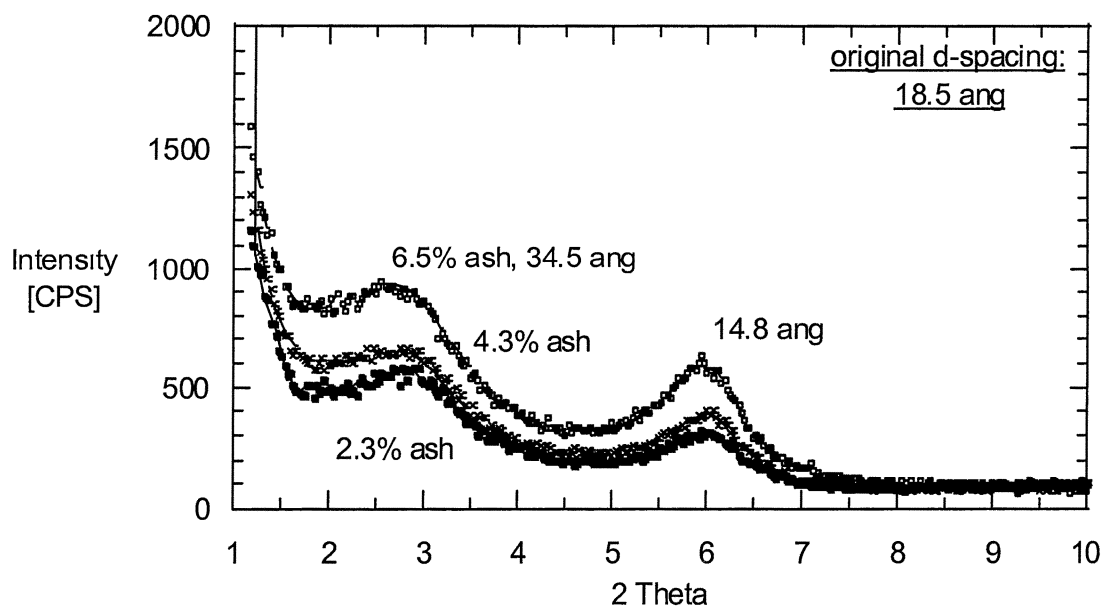


Figure 22. X-ray Diffraction Pattern for SAN/BM₂(HT) Blends

In addition, the effect of modulus enhancement for $(HE)_2MT$ clay blends with maleic anhydride (MA) vs acrylonitrile (AN) was studied. We believe that MA can work as a compatilizer to enhance exfoliation of $(HE)_2MT$ clay in SAN matrix, which could result in higher modulus enhancement. Three polymers used in this study are listed in Table 7. However, the results show (Figure 23) that clay blends with S/AN/MA

Table 7. Polymers used in the study of the effect of MA vs AN

Material	Description	Composition	Mw (g/mol)
Bayer, S/AN/MA	Styrene-acrylonitrile-maleic anhydride terpolymer	65% S, 1% MA, 34%AN	119400
Dow, SMA-8	Styrene-maleic anhydride copolymer	92% S, 8% MA	240000
Dow, SAN-25	Styrene-acrylonitrile copolymer	75% S, 25% AN	152000

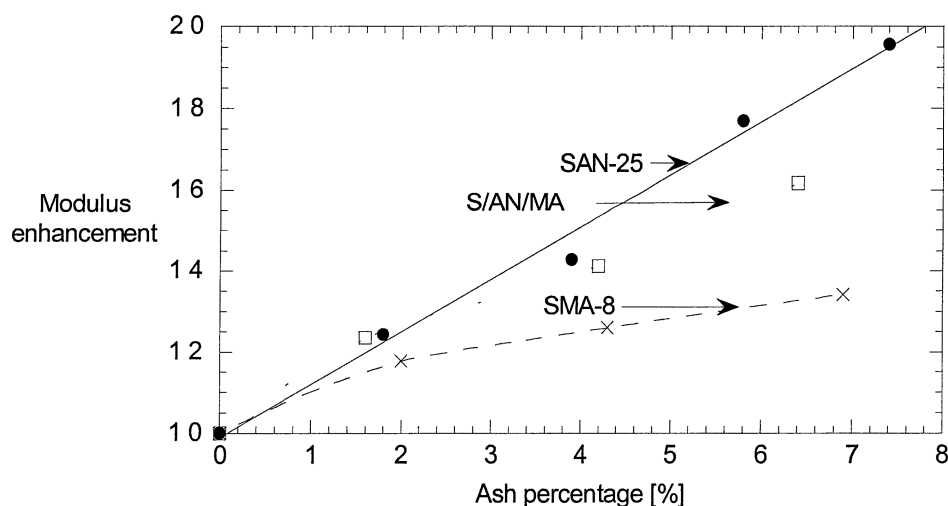


Figure 23. Comparison of Modulus Enhancement for $(HE)_2MT$ Clay Blended with SAN, S/AN/MA, and SMA-8

terpolymer or SMA-8 copolymer did not exhibit higher modulus enhancement compared to the clay blends with SAN copolymer, as expected. Tensile strength also dropped with the increasing of the amount of $(\text{HE})_2\text{MT}$ clay (Figure 24).

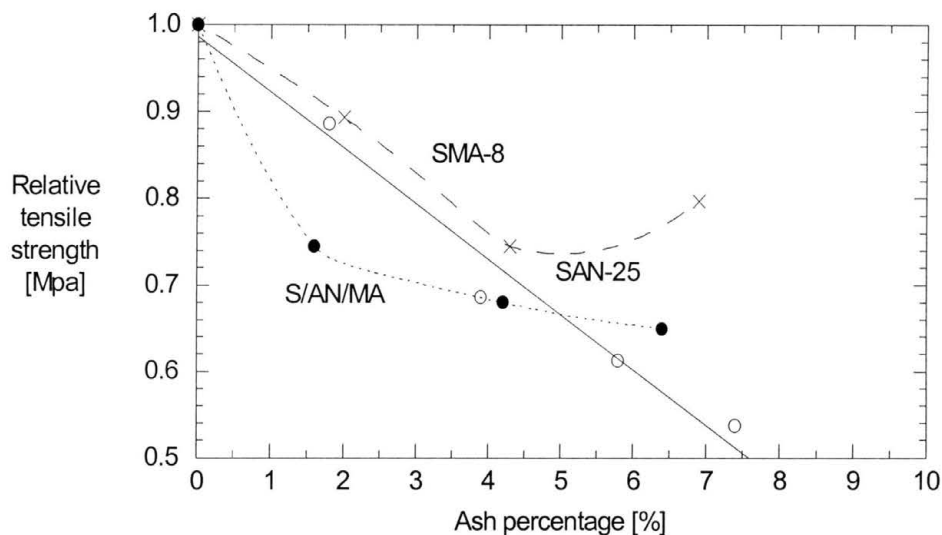


Figure 24. Comparison of Tensile Strength of $(\text{HE})_2\text{MT}$ Clay Blended with SAN, S/AN/MA, and SMA-8

Figure 25 shows the X-ray diffraction pattern for SMA-8/ $(\text{HE})_2\text{MT}$ clay blends. Three overlapping peaks were exhibited and no shift of the diffraction peak towards lower angle was detected. Therefore, we conclude that SMA-8/ $(\text{HE})_2\text{MT}$ clay exhibited phase-separated state due to non-expanded d-spacing change as discussed in section 2.3.3.

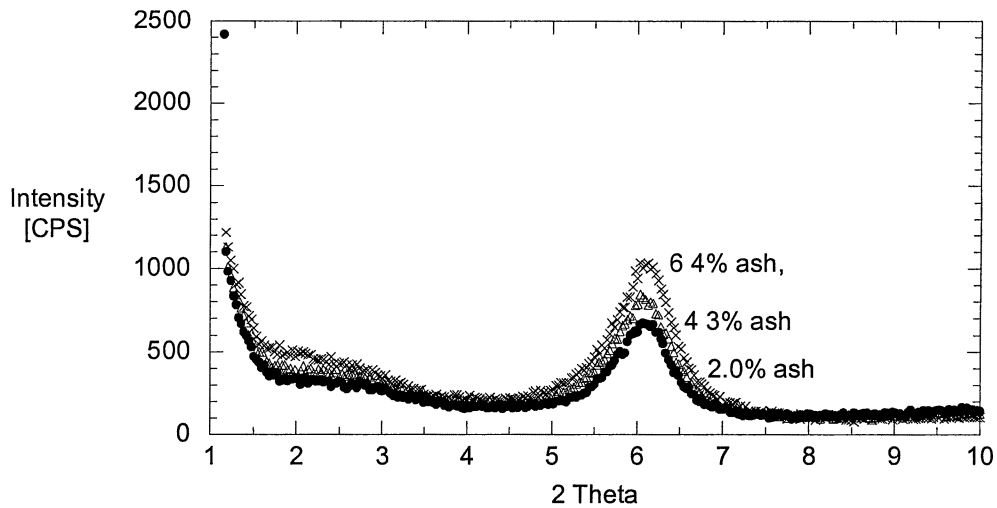


Figure 25. X-ray Diffraction Pattern for SMA-8/(HE)₂MT Blends

3.1.4 Flammability

3.1.4.1 Flammability of SAN vs Clay Type at Low Loading

The SAN/clay composite specimens were extruded to yield strands, which were chopped, dried and injection molded to result in test plaques. Three kinds of clay, (HE)₂MT, (HE)₂MC and BM₂(HT), were used in this study with about 2 % low ash loading. A summary of flammability test methods and requirements have been discussed in section 2.3.4. The plaques of the SAN/clay blends were placed under a heat flux of 35 kW/m² in the mass loss calorimeter for a test period of 900 seconds, and the resultant heat release rate (HRR) plots are shown in Figure 26. The peak value dropped just slightly with the ash loading at 1.8% for (HE)₂MT, 2.0% for (HE)₂MC and 2.4% for BM₂(HT), respectively.

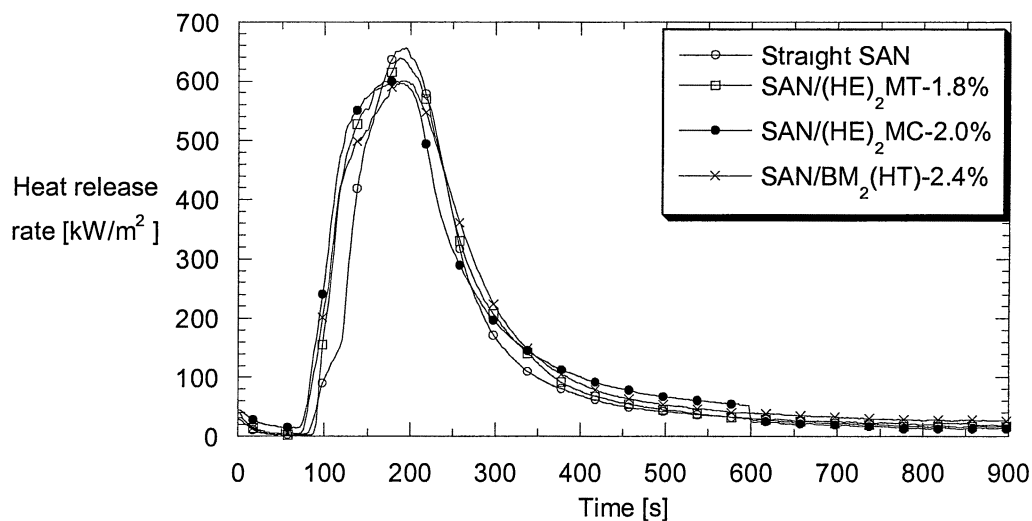


Figure 26. Plot of Heat Release Rate for SAN/Clay Blends at 35 kW/m^2

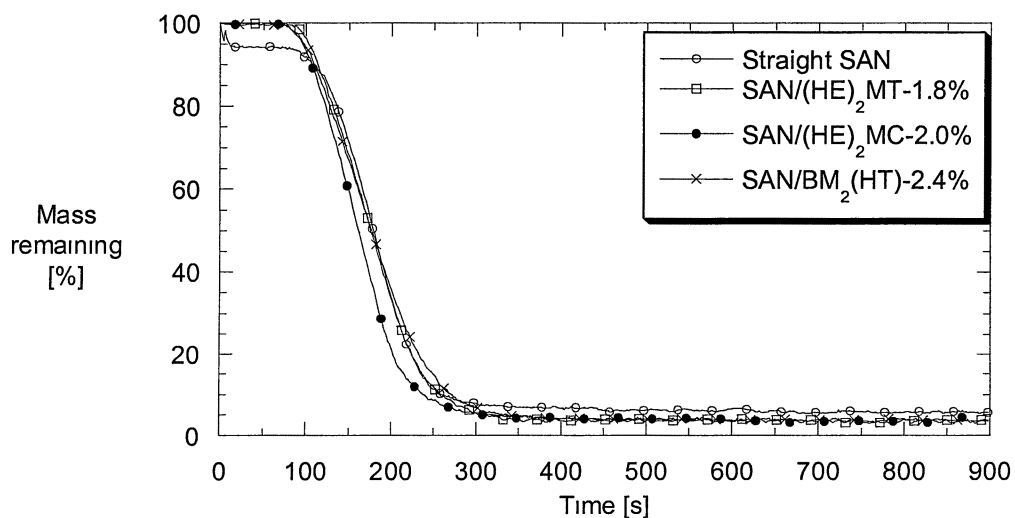


Figure 27. Plot of Residual Mass for SAN/Clay Blends at 35 kW/m^2

The plot of percent mass remaining percentage can be seen in Figure 27, as was the case in Figure 26. It reveals that these kinds of clay did not fire retard SAN polymer with small ash loading, which can also be demonstrated by detailed data collected from flammability tests (Table 8). The small reduction of PHRR shows only slight fire

retardancy. However, average HRR at 180s, time to ignition and time to peak all showed slightly undesirable trends for fire retardancy.

Table 8. Summary of Heat Release Rate Data at 35 kW/m² for SAN/Clay Blends

Material	PHRR (kW/m ²)	Avg. HRR at 180s (kW/m ²)	Time to Ignition (sec)	Time to Peak (sec)
Straight SAN	656	182	102	194
SAN/(HE) ₂ MT-1.8%	639	229	94	188
SAN/(HE) ₂ MC-2.0%	600	260	83	180
SAN/BM ₂ (HT)-2.4%	600	231	85	192

3.1.4.2 Flammability of SAN/(HE)₂MT vs Percent Ash

Previous flammability experiments reveal that clay may not fire retard SAN polymer at 2% low ash loading. In order to understand whether and how the content of the clay in the blends will effect the fire retardancy, we tested SAN/(HE)₂MT blends with varying percent ash. The reason (HE)₂MT clay was used in this study is that this kind of clay provides the best modulus enhancement, as demonstrated in section 3.1.2. The flammability test was conducted on SAN/(HE)₂MT blends with clay ash loading at 1.8%, 4.7% and 7.4%. The HRR plots are shown in Figure 28. The peak became broader and the peak height dropped with the increasing the amount of (HE)₂MT clay. The broader peak shape and lower peak value of the blends reveal that the rate of combustion for SAN/(HE)₂MT blends dropped with the increasing composition of the clay in blends compared to straight SAN.

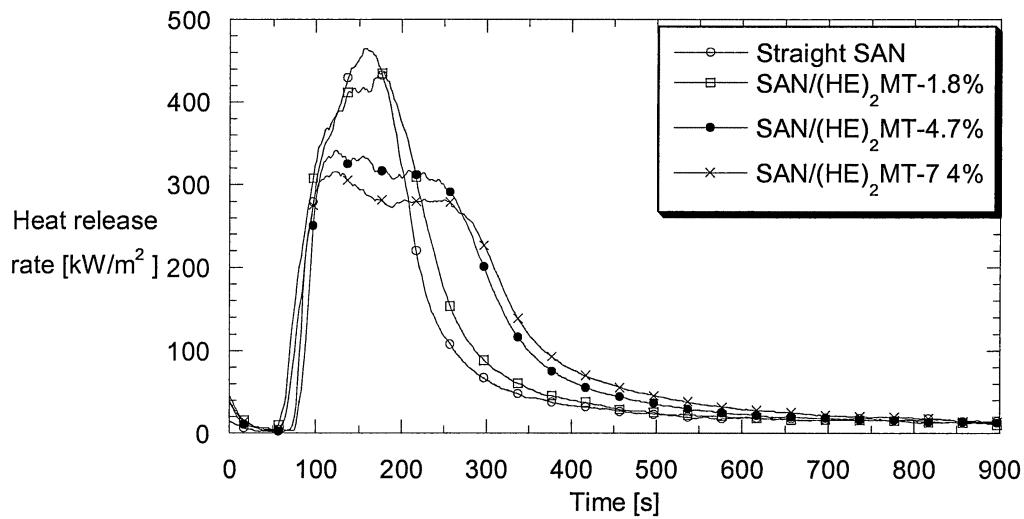


Figure 28. Plot of Heat Release Rate for SAN/(HE)₂MT Blends at 35 kW/m²

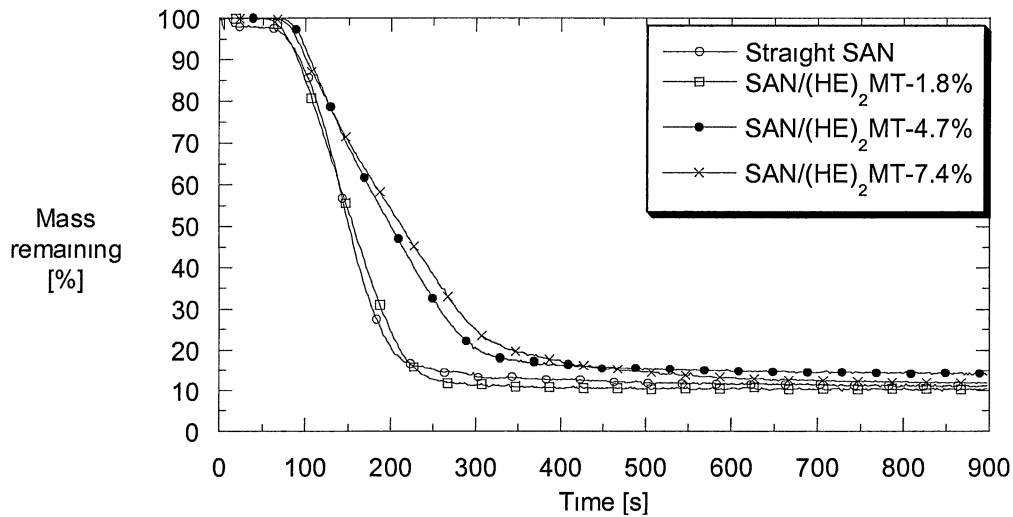


Figure 29. Plot of Residual Mass for SAN/(HE)₂MT Blends at 35 kW/m²

The mass remaining rate, represented by the slope of the curve, is shown in Figure 29. The steeper slope, of course, indicates a more rapid weight loss, and also a faster combustion rate. The results in Figure 29 reveal that mass loss rate was decreased with the increasing the amount of the clay as expected.

Figure 30 to 32 present clear trends in the improvement of the flame behavior for the SAN/(HE)₂MT blends. Figure 30 shows clearly that PHRR decreased with the increase of the loading of the clay. A 6%, 27% and 32% reduction in PHRR occurred with the ash loading of 1.8%, 4.7% and 7.4% (HE)₂MT clay, respectively. Figure 31 shows a slight change in AHRR at 180s with ash loading of 1.8%; however, a 25% reduction in AHRR resulted with maximum ash loading of 7.4%. Figure 32 shows time to ignition (TTI), a parameter of how quickly the material will ignite in a fire situation, is extended by 50% at ash loading over 4.7%. All these data are desirable for fire retardancy.

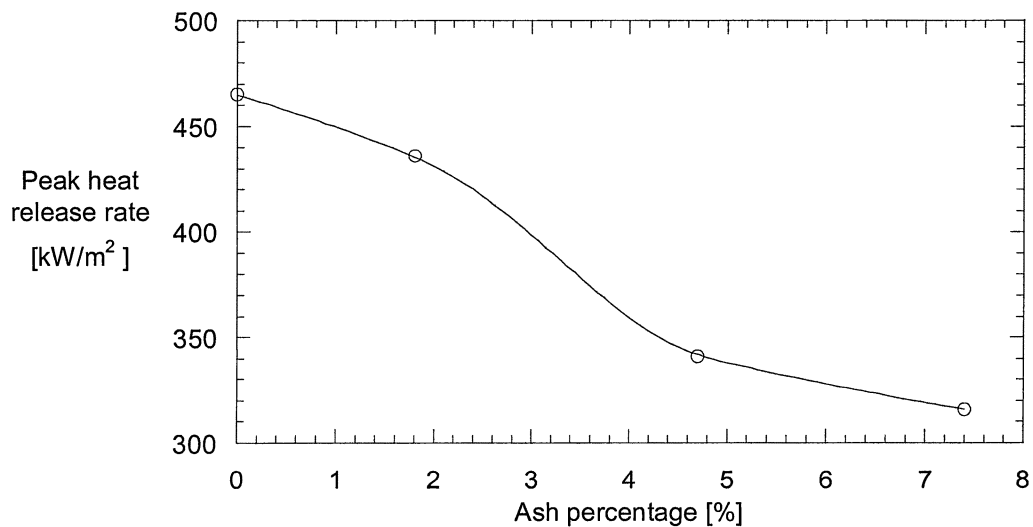


Figure 30. Plot of Peak Heat Release Rate for SAN/(HE)₂MT Blends at 35 kW/m²

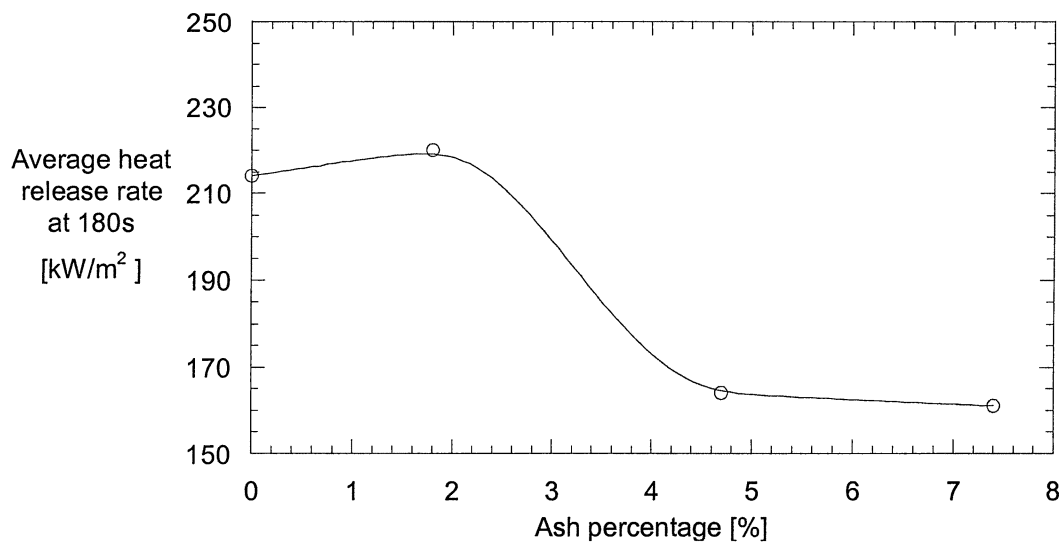


Figure 31. Plot of Average Heat Release Rate at 180s for SAN/(HT)₂MT Blends at 35 kW/m²

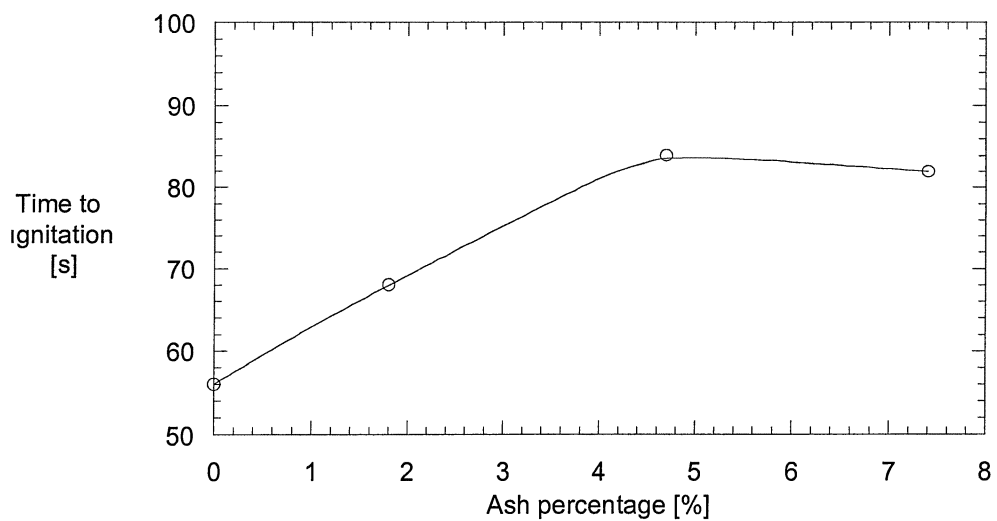


Figure 32. Plot of Time to Ignition for SAN/(HE)₂MT Blends at 35 kW/m²

3.2 Composition Study of ABS/Clay Blends

3.2.1 Tensile

Commercial ABS, Cycolac 5500, obtained from GE was used in this study. The material shipped by GE was black, but did not have any flame retardant additives. Two types of clay, $(HE)_2MT$ and $M_2(HT)_2-125$, were extruded with pure ABS polymer with varying ash percentages. Figure 33 shows that enhancement of Young's modulus for ABS/ $(HE)_2MT$ is higher than that of ABS/ $M_2(HT)_2-125$, matching the trends for these two clays used in the SAN model matrix as discussed in section 3.1.2. $(HE)_2MT$ clay increased modulus by 85% at ash loading of 8.6%, from 2.22 GPa to 4.10 GPa. $M_2(HT)_2-125$ clay increased the modulus by 38% at ash loading of 7.9%, from 2.22 GPa to 3.06 GPa. $(HE)_2MT$ showed an improved modulus enhancement for ABS polymer over $M_2(HT)_2-125$ as shown in Figure 34.

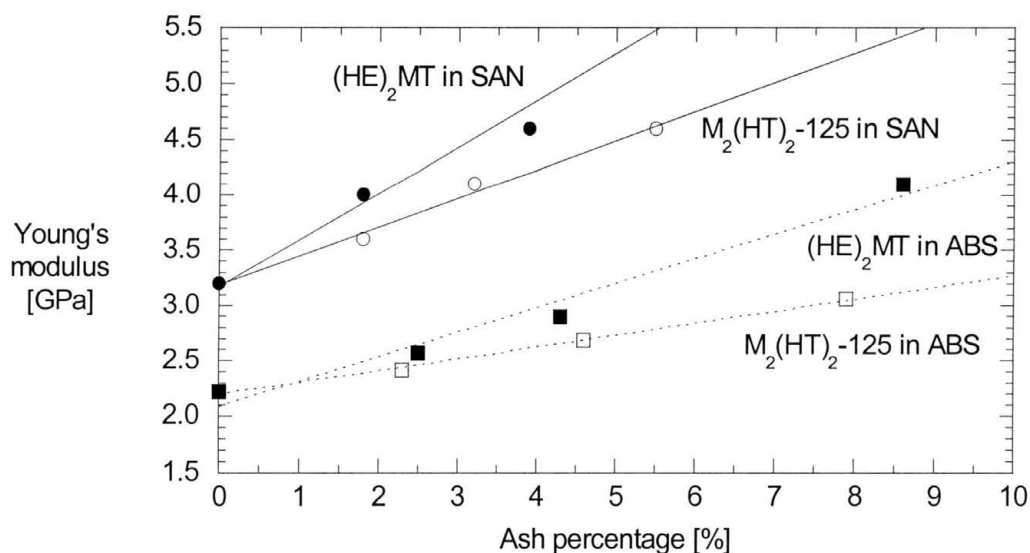


Figure 33. Comparison of Young's Modulus for ABS/Clay and SAN/Clay Blends

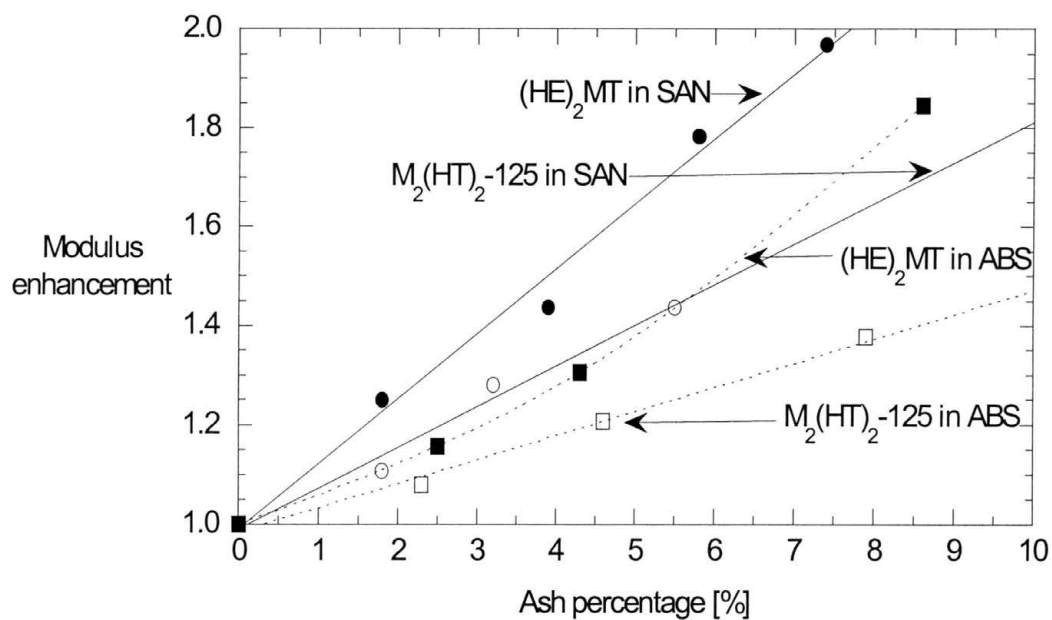


Figure 34. Comparison of Modulus Enhancement for ABS/Clay and SAN/Clay Blends

Figure 35 shows the original tensile stress/strain diagram for ABS/(HE)₂MT blends. There is no yield point exhibited through the ABS/clay tensile test, probably because the amount of the rubber is not enough to exhibit yielding behavior; but some stress whitening was observed, indicating a trend towards more ductile-like behavior on addition of rubber.

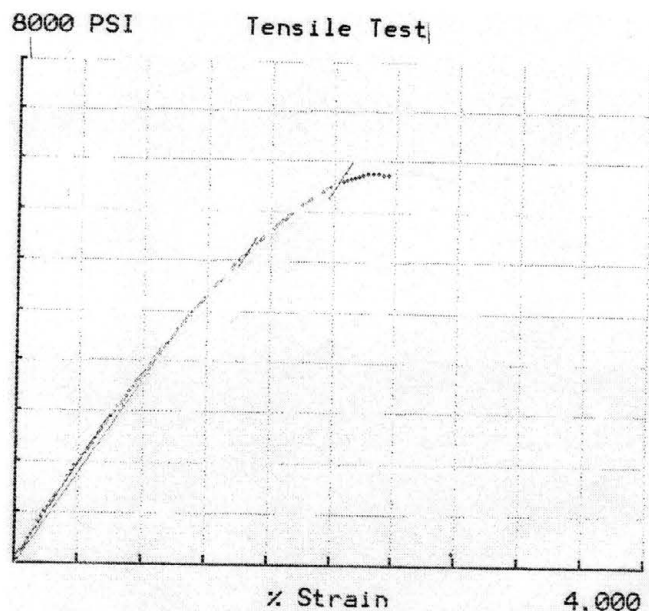


Figure 35. Stress/strain Diagram for ABS/(HE)₂MT Blends at 14% Rubber Content

Figures 36 and 37 show that tensile strength decreased with an increasing amount of clay, but the decrease was not as significant as that seen in SAN. It is important that the loss in tensile strength caused by addition of clay was mediated by addition of rubber; obviously there is a trade-off in modulus enhancement. Optimization for a given application, then, would depend on the properties required, and one would then “tune” the percent clay and percent rubber to achieve that target.

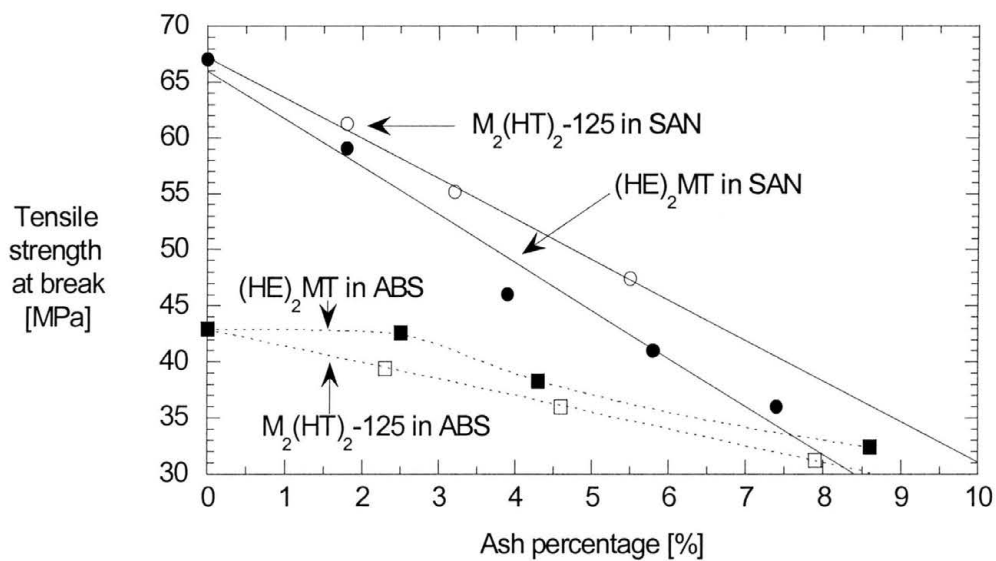


Figure 36. Comparison of Tensile Strength at Break Point for ABS/Clay and SAN/Clay Blends

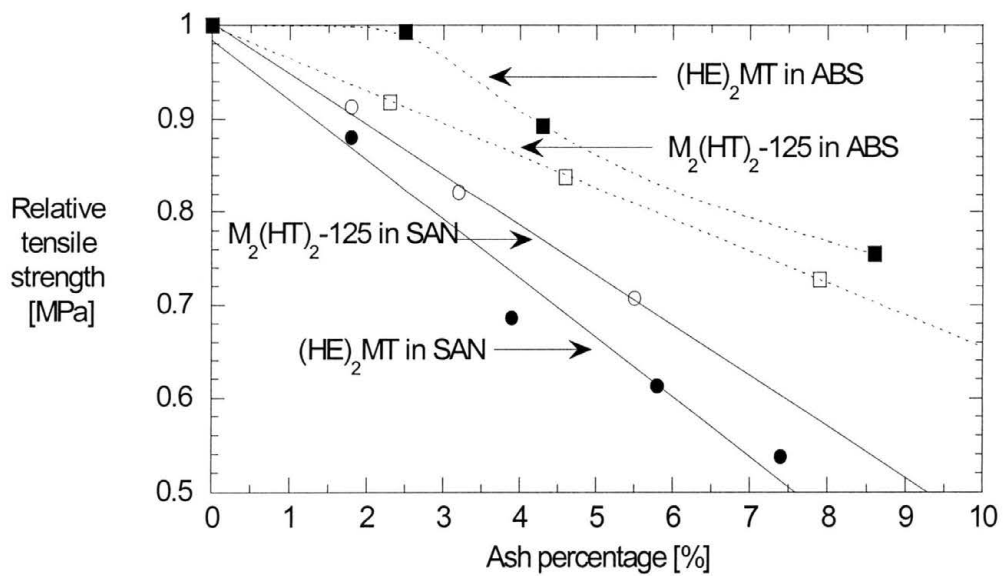


Figure 37. Relative Tensile Strength at Break Point for ABS/Clay and SAN/Clay Blends

Figure 38 shows the results of the elongation-at-break on samples of ABS/clay blends. The elongation is reduced at almost the same rate for the two ABS/clay blends as ash percentage increased. Obviously, the significant reduction of elongation resulted in lack of enough rubber present in ABS system to allow the blend to yield.

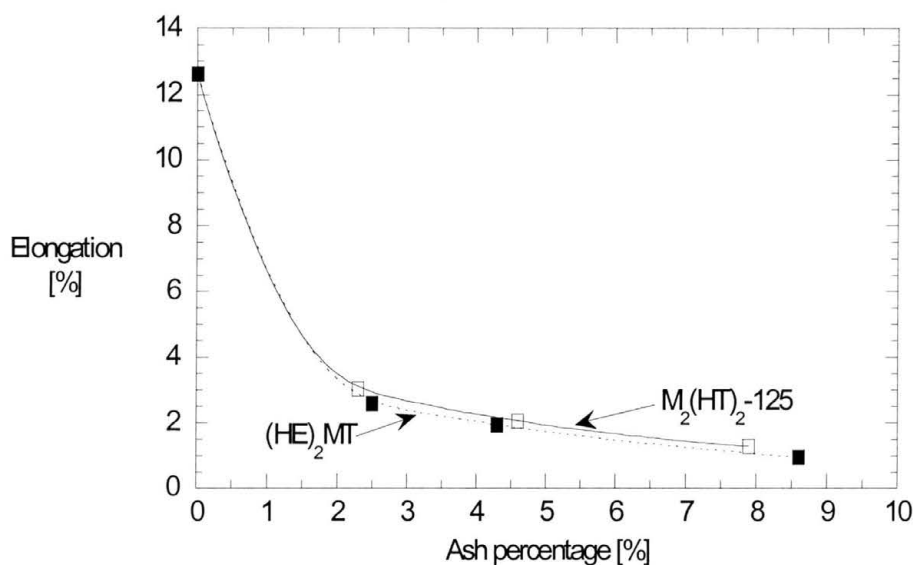


Figure 38. Elongation of ABS/Clay Blends

3.2.2 Notched Izod Impact

The Notched Izod impact strengths of ABS/clay blends are summarized in Figure 39. The results show that the impact strength dropped significantly with the addition of the small amount of clay. The decrease of the impact strength can be attributed to interaction between polymer chain and MMT clay, which makes the rubber particle in blends less mobile to dissipate impact energy compared to the rubber particle in straight ABS. By extrapolation of our control curve of rubber-grafted SAN/straight SAN blends in Figure 55, the GE ABS contains approximately 14% rubber. We can get the 120 J/m of this

virgin GE blend in a rubber-grafted SAN/SAN/clay blends at 2% ash of clay by adding up to around 29% rubber.

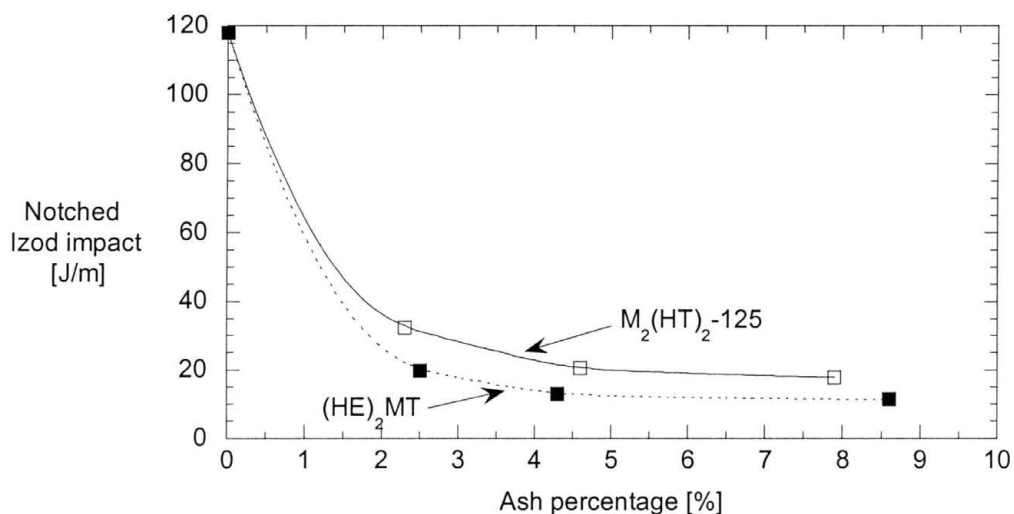


Figure 39. Notched Izod Impact (J/m) for ABS/Clay Blends

3.2.3 X-ray Diffraction Pattern of the Blends

Figure 40 shows XRD patterns for ABS/ $M_2(HT)_2-125$ blends, indicating a high level of intercalated order by the three overlapped peaks. Figure 41 shows XRD for ABS/ $(HE)_2MT$ blends. Less order (only 2 clear peaks) and a gradually climbing baseline indicate light exfoliation and some intercalation. These two XRD patterns match quite well with the two XRD patterns for SAN/ $M_2(HT)_2-125$ and SAN/ $(HE)_2MT$ blends discussed in section 3.1.3, indicating a small amount of rubber content (~14%) does not change the state of the intercalation of the nanocomposite.

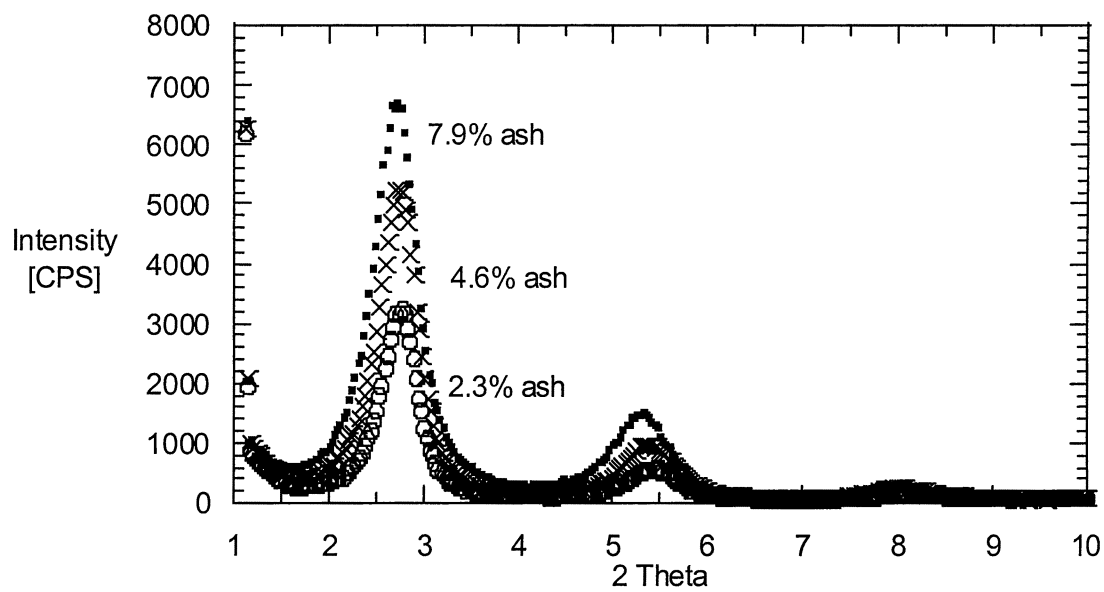


Figure 40. X-ray Diffraction Pattern for ABS/M₂(HT)₂-125

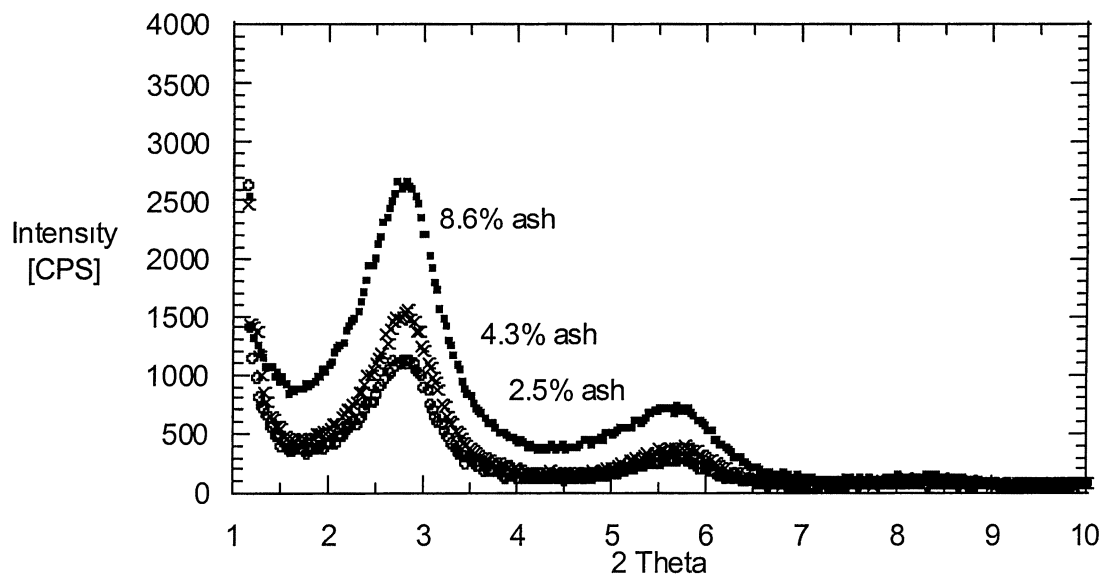


Figure 41. X-ray Diffraction Pattern for ABS/(HE)₂MT

3.2.4 Flammability

Commercial montmorillonite clays have been shown to fire retard several polymer systems when the clay is either exfoliated or intercalated. In order to establish feasibility of this additive as a fire retardant in application of commercial ABS (GE Cyclocac 5500), we tested two types commercial clay, $(\text{HE})_2\text{MT}$ and $\text{M}_2(\text{HT})_2-125$, with the weight loading at 0, 5, 8.5 and 12.5% respectively. As shown in Figure 42 for ABS/ $(\text{HE})_2\text{MT}$ blends, the peak shape became broader and peak height became lower with a higher amount of clay loading. The time-to-peak also shifted toward longer times with the higher amount of clay loading. As shown in Figure 43, the remaining mass percentage of ABS/ $(\text{HE})_2\text{MT}$ blends becomes higher with the higher amount of clay loading. All of the above-mentioned changes are desirable results we want to achieve for the fire retardancy. The flammability test results for ABS/ $\text{M}_2(\text{HT})_2-125$ in Figure 44 and 45 showed the same trends as did for ABS/ $(\text{HE})_2\text{MT}$ in Figure 42 and 43.

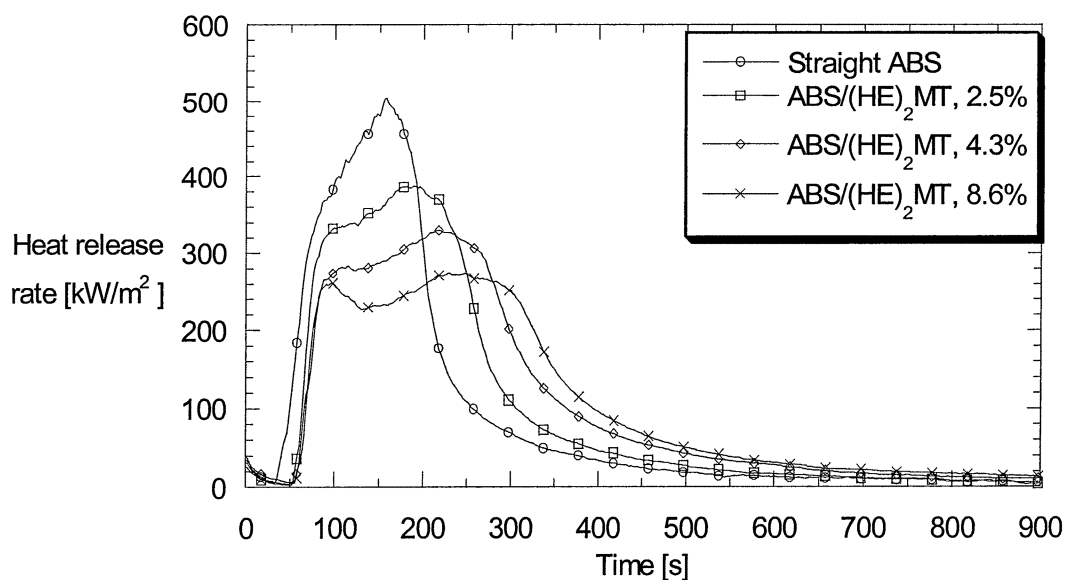


Figure 42. Plot of Heat Release Rate for ABS/ $(\text{HT})_2\text{MT}$ at 35 kW/m^2

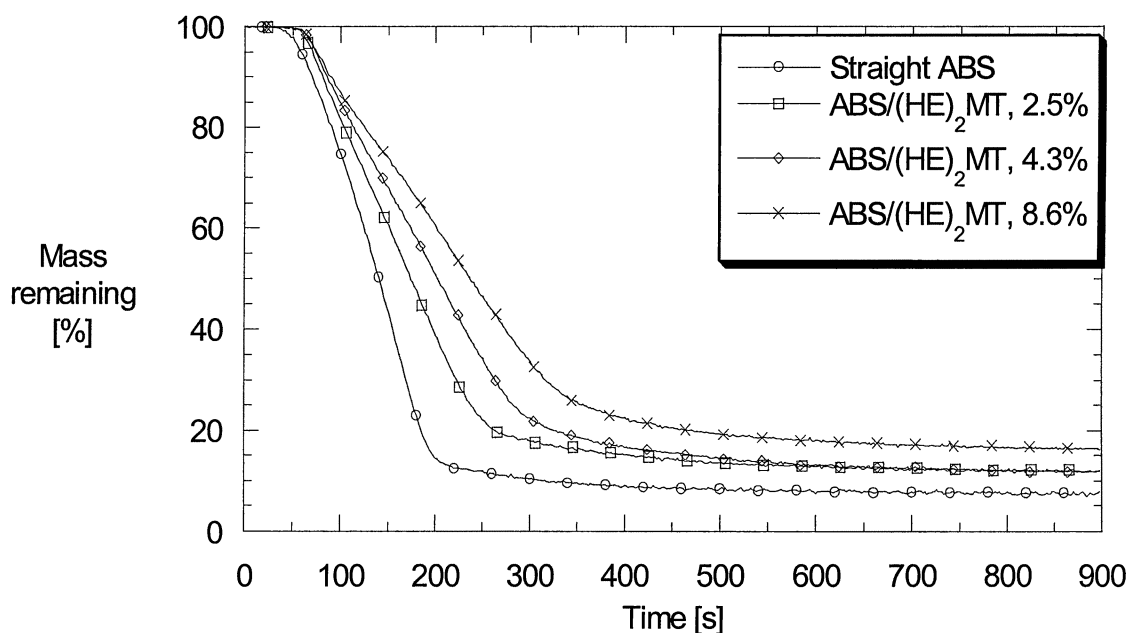


Figure 43. Plot of Residual Mass for ABS/(HT)₂MT Blends at 35 kW/m²

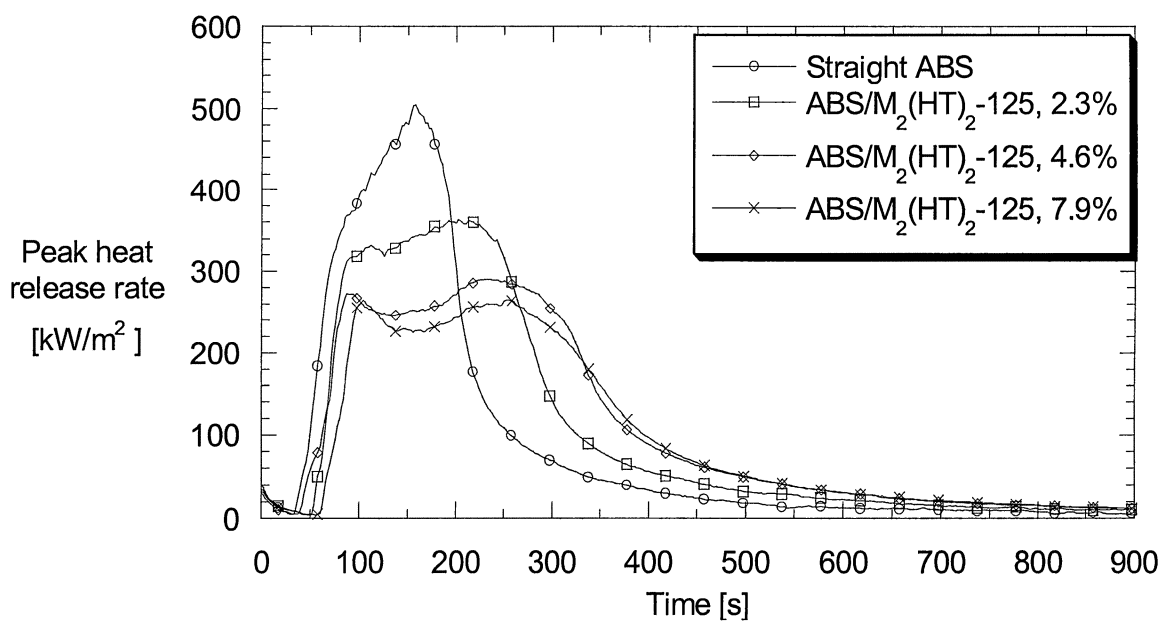


Figure 44. Plot of Peak Heat Release Rate for ABS/M₂(HT)₂-125 Blends at 35 kW/m²

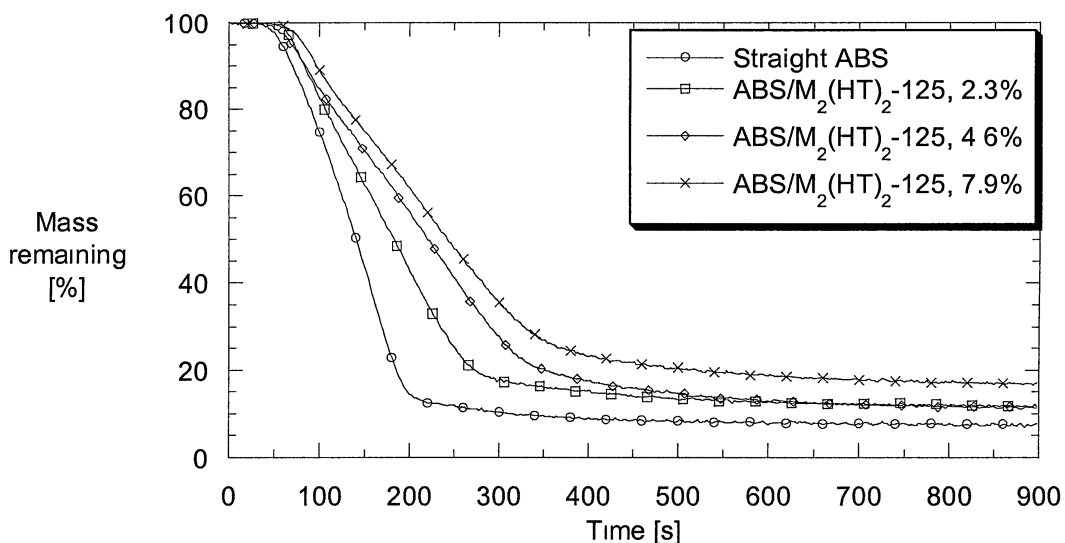


Figure 45. Plot of Residual Mass Rate for ABS/ M₂(HT)₂-125 Blends

Figures 46 to 50 present a more quantitative comparison of the flammability improvement. As shown in these figures, the two different types of clay show the same trends in fire retardancy. Improvement of fire retardance has been proposed to be due to the tortuous pathway formed in nanocomposites discussed in section 1.1, which slows the combustion speed, as well as possible thermal insulation of the char.

Figure 46 shows that (HE)₂MT clay dropped the PHRR of ABS by 46% at 8.6% ash loading, from 505 kW/m² to 274 kW/m²; M₂(HT)₂-125 clay performed similarly by decreasing PHRR by 48% at 7.9% ash loading, from 505 kW/m² to 265 kW/m². Figure 47 shows that (HE)₂MT clay at 8.6% ash loading in ABS dropped average HRR at 180s by 48% compared to ABS, from 292 kW/m² to 151 kW/m²; M₂(HT)₂-125 clay behaved similarly (53% decrease in average HRR at 7.9% ash loading, from 192 kW/m² to 151 kW/m²). The significant drop of PHRR and average HRR at 180s reveals that combustion speed dropped significantly, as expected.

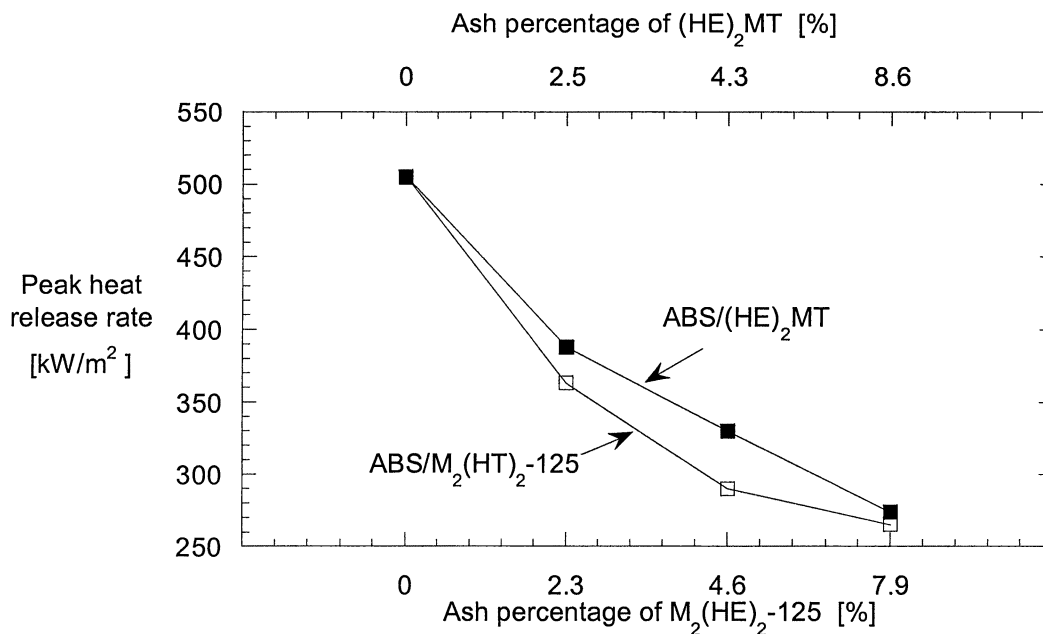


Figure 46. Comparison of Peak Heat Release Rate for ABS/Clay Blends

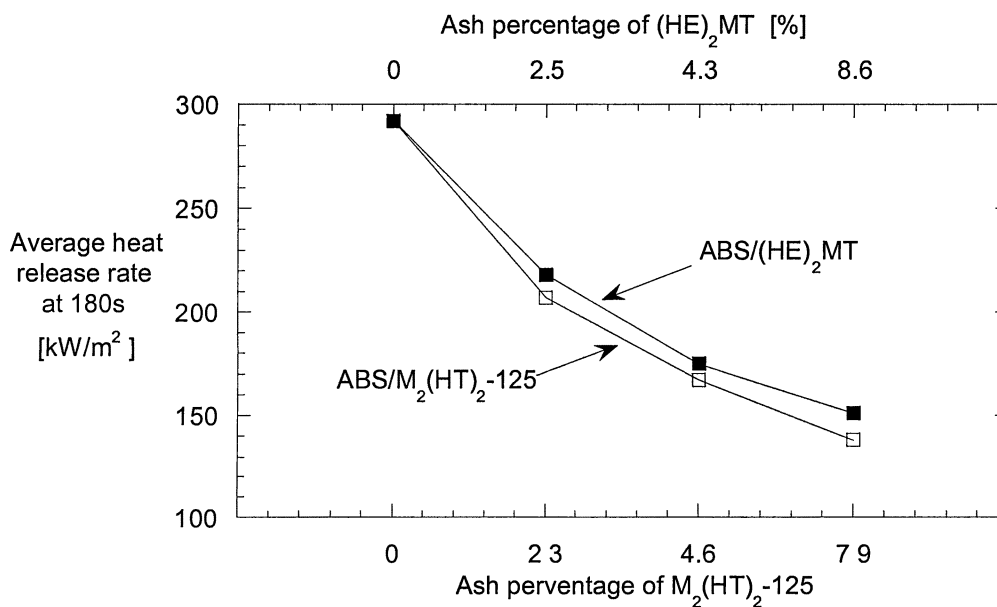


Figure 47. Comparison of Average Heat Release Rate at 180s for ABS/Clay Blends

Figure 48 shows that (HE)₂MT clay extended time-to-peak by 61% for ABS system at 8.6% ash loading; M₂(HT)₂-125 clay performed similarly (46% extended time-to-peak at 7.9% ash loading). Figure 49 shows (HE)₂MT clay extended time to ignition by 78% at 8.6% ash loading; M₂(HT)₂-125 clay gave similar results (103% extended time to ignition

at 7.9% ash loading). Those two extended time parameters, as we expected, mean that people can have a longer time to escape from hazardous structure fires. Figure 50 shows that $(\text{HE})_2\text{MT}$ clay increased residual mass by 142% at 8.6% ash loading;

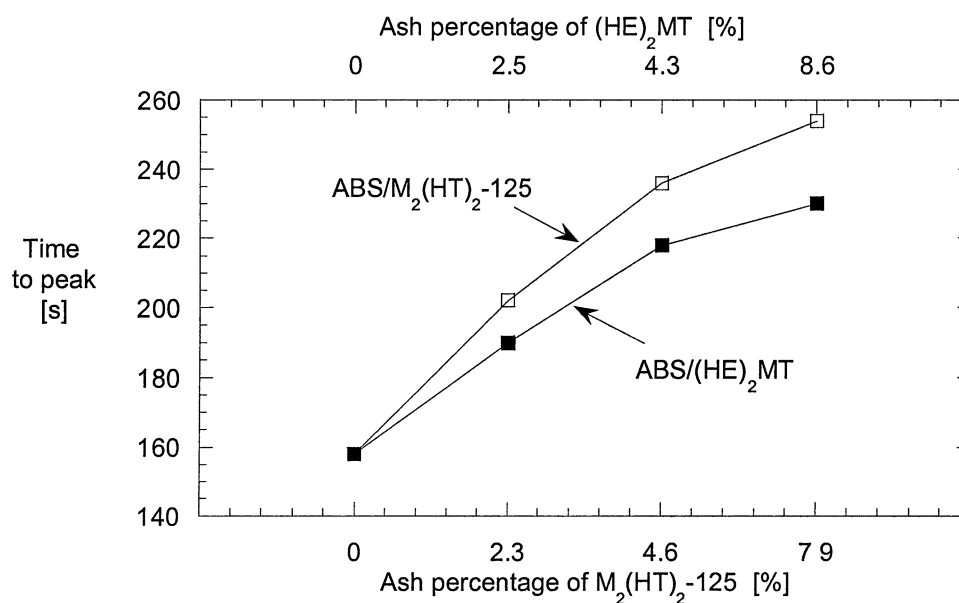


Figure 48. Comparison of Time to Peak for ABS/Clay Blends

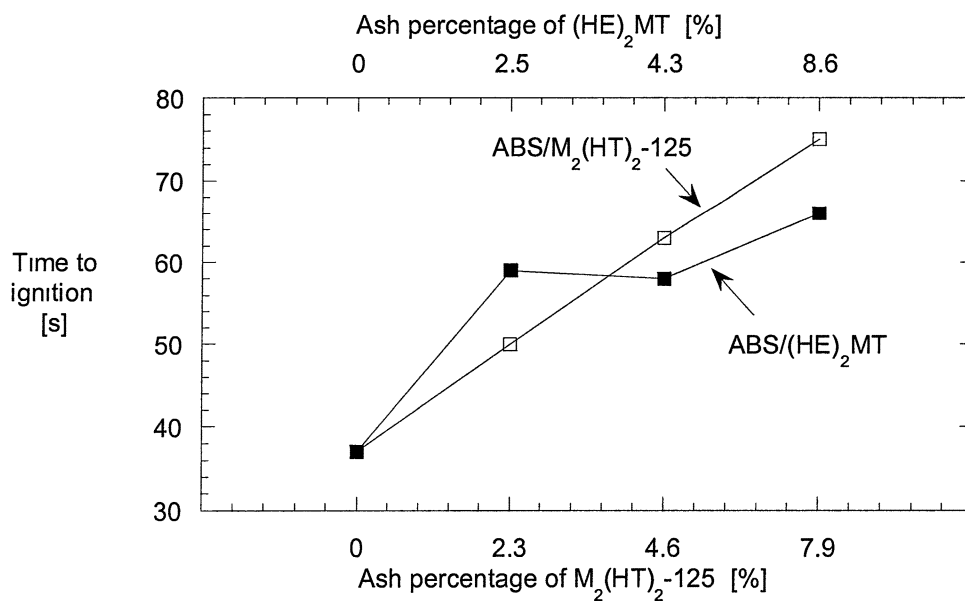


Figure 49. Comparison of Time to Ignition for ABS/Clay Blends

$M_2(\text{HT})_2-125$ clay likewise (103% increased residual mass at 7.9% ash loading). The higher residual mass can serve as an insulator to slow the spread of the fire.

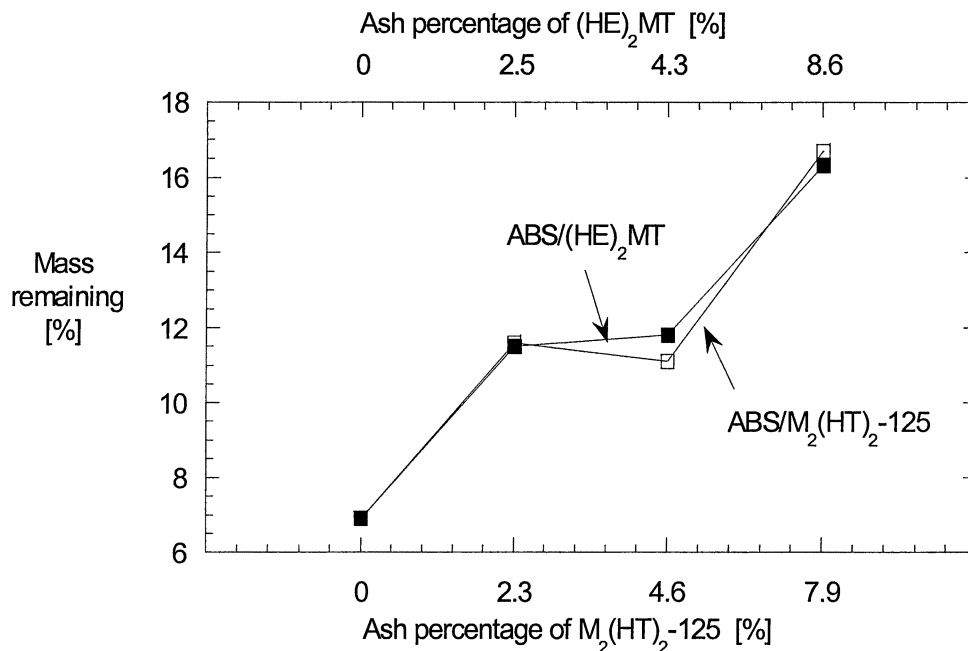


Figure 50. Comparison of Residual Mass for ABS/Clay Blends

3.3 Processing Sequence Study of ABS/Clay Blends

We incorporated clay into an ABS system in two ways in order to understand how the processing sequence affects the properties of ABS/clay blends. First was simultaneous processing in which the SAN matrix, rubber-grafted SAN and $(\text{HE})_2\text{MT}$ clay were extruded simultaneously. Second was non-simultaneous processing, in which rubber-grafted SAN was added to the SAN/ $(\text{HE})_2\text{MT}$ masterbatch in a second extrusion step. Since a higher viscosity matrix like SAN can exfoliate the clay more efficiently compared to ABS matrix, we explored the possibility of producing a masterbatch of SAN/clay, to be “let down” with a rubber concentrate.

3.3.1 Tensile

Figure 51 shows that the Young's modulus dropped with an increasing amount of the rubber percentage in ABS system no matter whether the system contained clay or not. It also reveals that $(HE)_2MT$ clay at 2-3% ash loading slightly improved the modulus with either simultaneous or masterbatch processing. No significant differences in modulus were noted between the two processing methods. Figure 52 shows that the tensile strength decreased with an increasing amount of rubber percentage, either with or without the clay. It also reveals that a small amount of clay for either processing method did not alter the results of tensile strength. The yield behavior (Figure 53) is due to the amount of rubber (from 22.5% to 27%) which is sufficient to produce yielding.

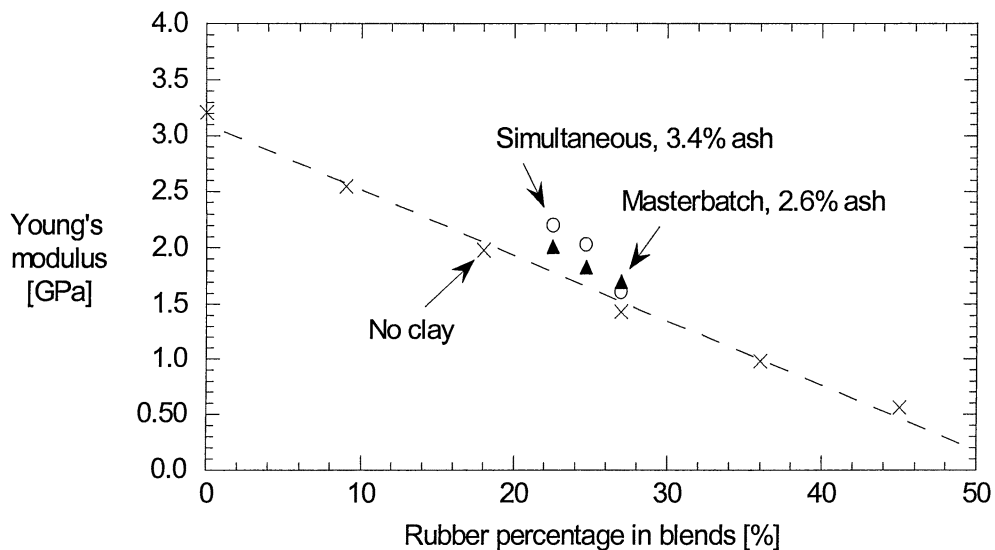


Figure 51. Young's Modulus for Simultaneous vs Masterbatch ABS/Clay

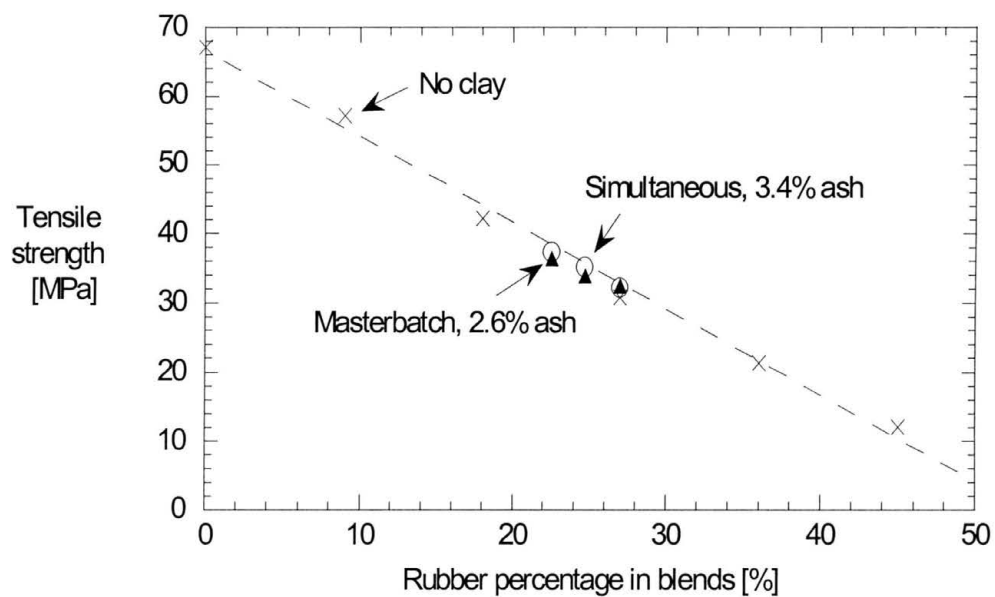


Figure 52. Tensile Strength for Simultaneous vs Masterbatch ABS/Clay Blends

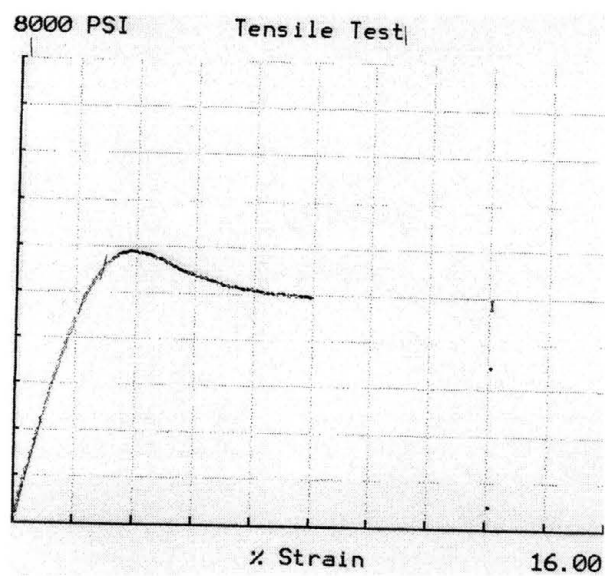


Figure 53. Stress/strain Diagram for ABS/(HE)₂MT Blends at 22.5% Rubber Content

Figure 54 shows that elongation dramatically dropped with the loading of a small amount of clay for either processing method, since probably non-exfoliated tactoids can form stress-concentration points. The drop of elongation also contributes to a trade-off between clay and rubber content.

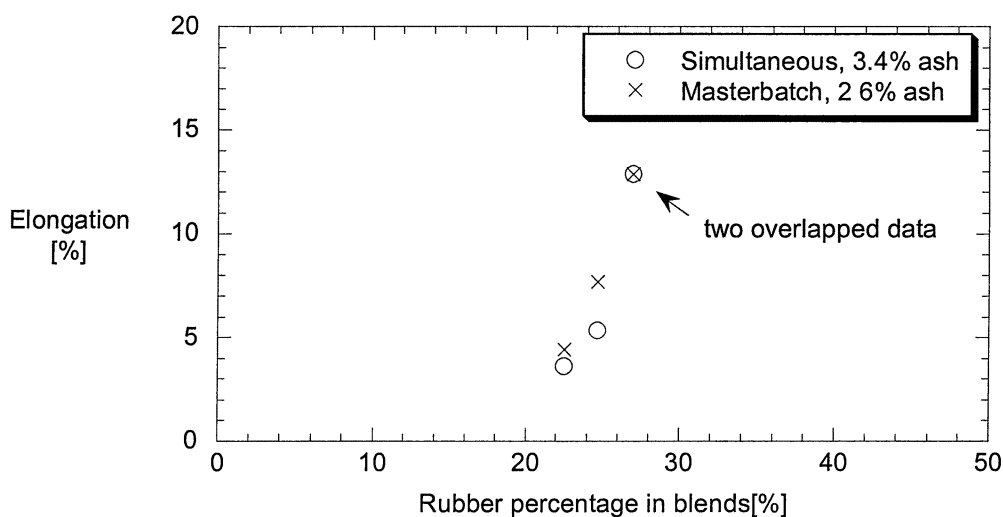


Figure 54. Elongation for Simultaneous vs Masterbatch ABS/Clay Blends

3.3.2 Notched Izod Impact

Notched Izod impact strengths are shown in Figure 55 as a function of rubber content. An optimum impact strength at about 28% rubber appeared in the virgin ABS as the rubber percentage was varied. The impact strength dropped dramatically with the loading of a small amount of clay by either simultaneous or masterbatch processing. This figure also shows that increased rubber content can improve the impact strength of the clay-filled ABS system.

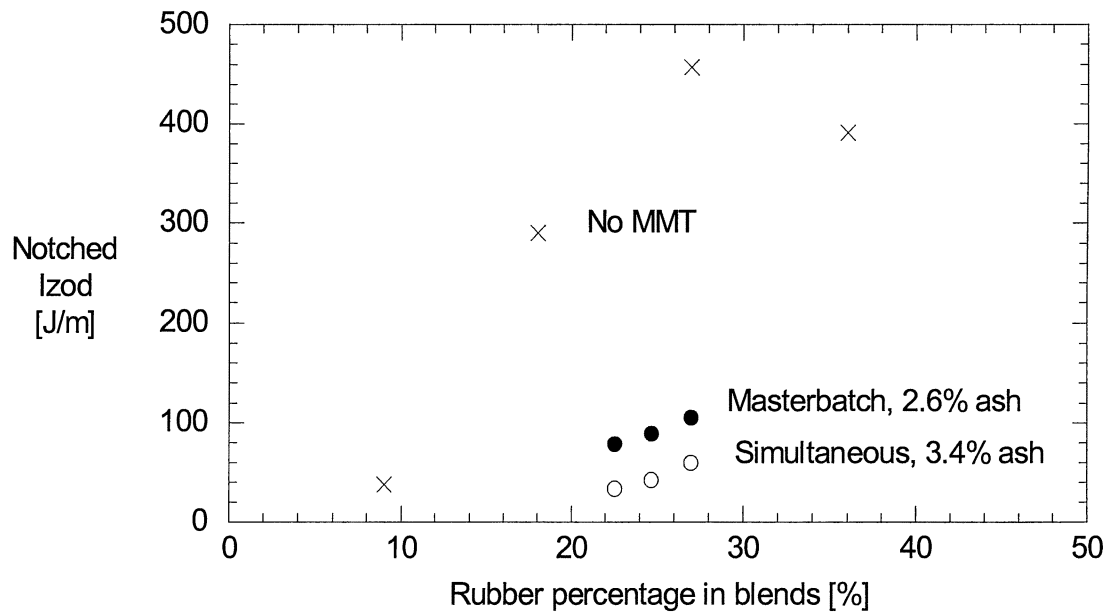
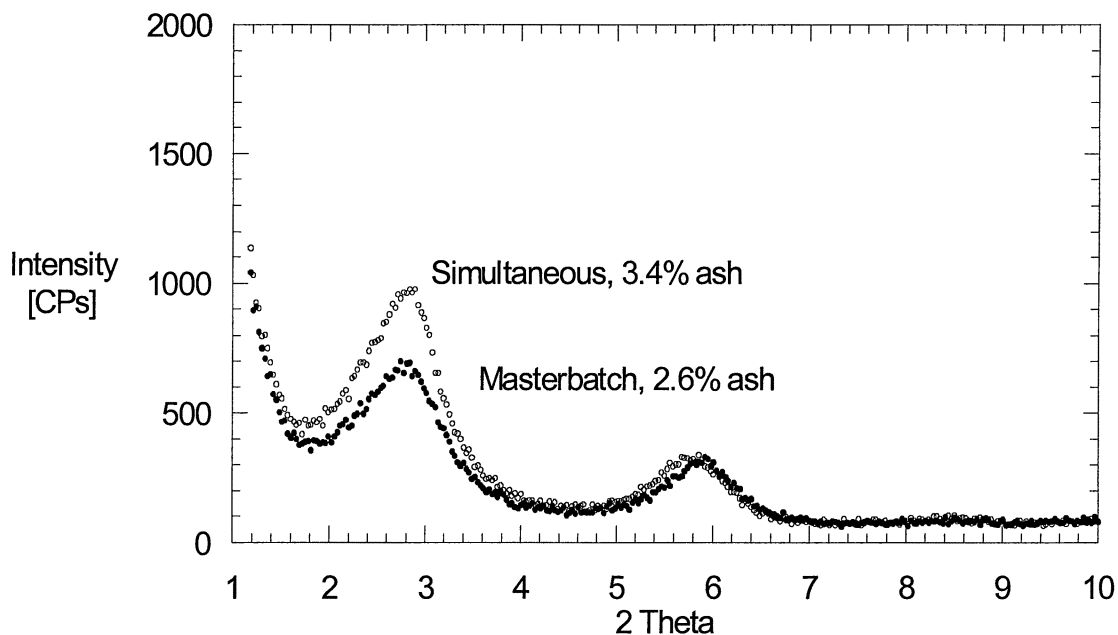


Figure 55. Impact Test Results for Simultaneous vs Masterbatch ABS/Clay Blends

3.3.3 X-ray Diffraction Pattern

The XRD pattern (Figure 56) shows that the two peaks of simultaneous blends overlap well with the two peaks of masterbatch blends. Their gradually climbing baselines also overlap quite well. It reveals that simultaneous processing probably made the same morphology of intercalated state for the clay-filled ABS system as the masterbatch processing did. Absolute values of peak height varied due to the different ash percentage.



**Figure 56. X-ray Diffraction Pattern
for Simultaneous vs Masterbatch ABS/Clay Blends**

3.3.4 Flammability

In order to understand whether processing sequence will affect fire retardance, we tested simultaneous and masterbatch ABS/SAN/(HE)₂MT blends in the mass loss calorimeter. Figure 57 shows that the curves of heat release rate for five different composition blends are almost congruent, and Figure 58 also shows the overlapped curves of mass remaining rate for the five blends. It reveals that difference in processing method, simultaneous vs masterbatch method, did not result in differences in fire retardance. It also shows that small variations in rubber content ($\pm 5\%$) with the same clay content did not affect fire retardant behavior significantly.

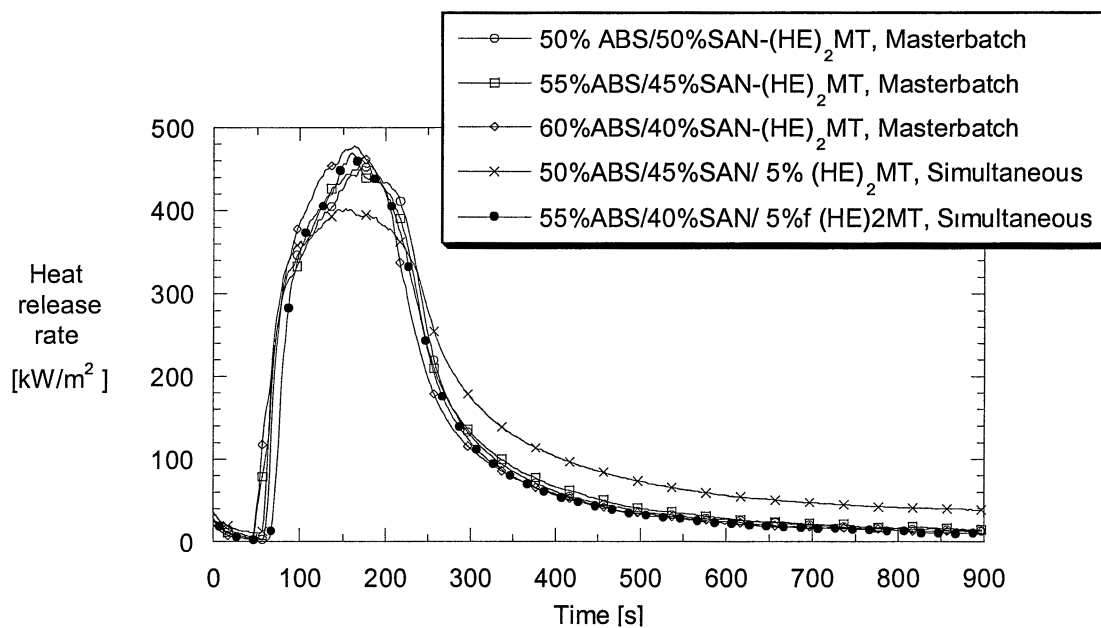


Figure 57. Comparison of Heat Release Rate at 35 kW/m^2 for Simultaneous vs Masterbatch ABS/SAN/Clay Blends

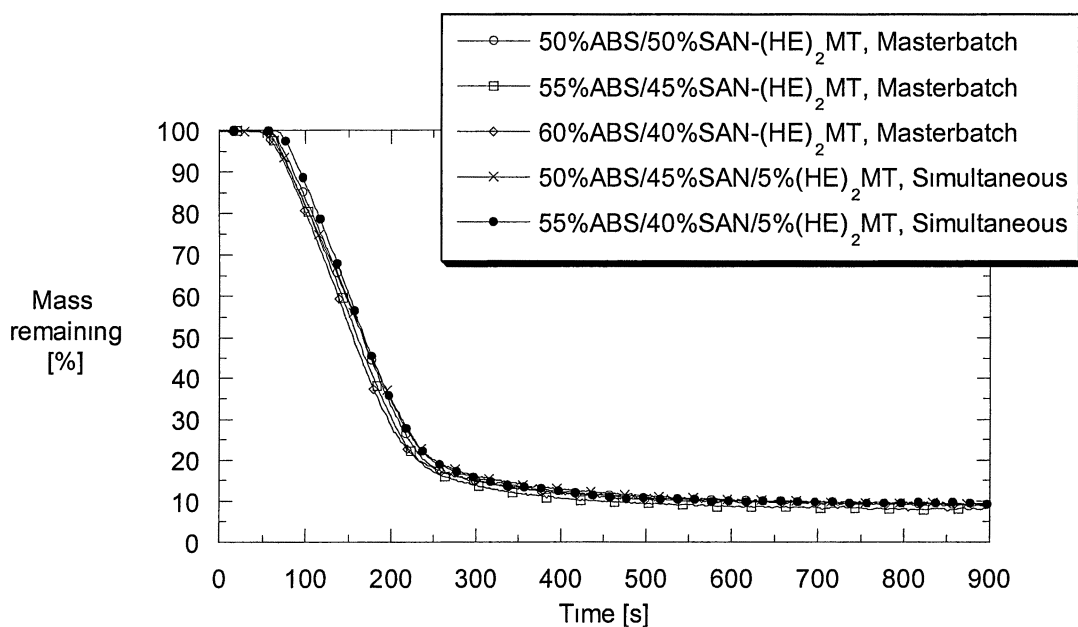


Figure 58. Comparison of Residual Mass at 35 kW/m^2 for Simultaneous vs Masterbatch ABS/SAN/Clay Blends

4.0 CONCLUSION

Montmorillonite clay, a non-halogenated fire retardant was studied to fire retard acrylonitrile-butadiene-styrene (ABS) system *via* melt processing. Potential trade-offs between mechanical properties *vs* fire retardancy for ABS/clay blends were investigated. Styrene-acrylonitrile (SAN), a model polymer matrix for ABS system, blended with five types of montmorillonite (MMT) clay surface-treated by quaternary ammonium ions, was investigated in order to recognize the compatibility and therefore dispersion of the organic filler in the melt. The results can be summarized in the following three major investigations.

The first investigation dealt with the incorporation of five types of MMT clay into SAN matrix. X-ray diffraction demonstrated that either an unintercalated phase or hybrid phase (combination of intercalated and exfoliated phase) were obtained for these SAN/clay blends. (HE)₂MT clay blends exhibited the best combination of mechanical properties, indicating the best exfoliation, compared to four other clays. (HE)₂MT clay blends contributed to the highest modulus enhancement in the SAN/clay blend over four other clays, increasing the modulus by 20% over straight SAN at the 2% ash loading level. In comparison, a fully exfoliated, well-compatibilized nylon/clay blend produced on the same extruder by colleagues at UT showed a 40% enhancement in modulus at 2% ash loading. All five types of clay dropped the blend tensile strength significantly. (HE)₂MT clay decreased tensile strength by 14% to at 2.0% ash loading over straight

SAN. Tensile strength of polymer/clay blends for ductile polymers generally increase. This contrary behavior in a brittle SAN/clay matrix is assumed to be caused by fracture mechanisms that differ for ductile or brittle blends

In the first investigation, three of above-mentioned five surface-treated clays at about 2% small ash loading were studied to fire retard the SAN matrix. No fire retardant behavior was observed, since two major factors, peak heat release rate and average heat release rate at 180 seconds were not noticeably reduced. $(\text{HE})_2\text{MT}$ clay was incorporated into SAN matrix at 1.8, 4.7, and 7.4% ash loading in order to investigate this further. The results exhibited the trends that fire retardancy were significantly improved at loadings greater than 2% ash, with lower PHRR on increasing the amount of $(\text{HE})_2\text{MT}$ clay in the SAN matrix. $(\text{HE})_2\text{MT}$ clay at 7.4% ash loading decreased PHRR by 32%, from 465 kW/m^2 to 316 kW/m^2 ; and decreased AHRR by 25%, from 214 kW/m^2 to 161 kW/m^2 .

The second investigation dealt with the incorporation of MMT clay into commercial ABS. Two types of surface-treated clay, $(\text{HE})_2\text{MT}$ and $\text{M}_2(\text{HT})_2\text{-125}$, were used in this study. Either $(\text{HE})_2\text{MT}$ or $\text{M}_2(\text{HT})_2\text{-125}$ clay showed improvement of fire retardancy to ABS system. $(\text{HE})_2\text{MT}$ clay at 8.6% ash loading decreased PHRR by 46%, from 505 kW/m^2 to 274 kW/m^2 ; it also decreased AHRR by 48%, from 292 kW/m^2 to 151 kW/m^2 . $\text{M}_2(\text{HT})_2\text{-125}$ clay at 7.9% ash loading decreases PHRR by 48%, from 505 kW/m^2 to 265 kW/m^2 and decreases AHRR by 53%, from 292 kW/m^2 to 138 kW/m^2 . This reduction in PHRR and AHRR was a nonlinear decreasing function of clay loading. $(\text{HE})_2\text{MT}$ clay exhibited a higher modulus enhancement than $\text{M}_2(\text{HT})_2\text{-125}$ clay did for the ABS system, and this trend correlated to that seen for SAN/clay blends. $(\text{HE})_2\text{MT}$ clay at 8.6% ash loading increased ABS modulus by 85%. The slope of modulus enhancement vs ash

loading for the SAN blends was higher than that for ABS blends provided by either clay, and this is presumed to be due to better melt exfoliation because the shear developed by extruder for higher melt viscosity SAN was greater than the shear developed while extruding ABS. If the rubber content is high enough, we can maintain virgin tensile strength even in presence of clay; also ductile behavior and yielding have been shown, even in the presence of clay. Further, notched Izod impact strength dropped significantly with the addition of either of the two clays into ABS system. (HE)₂MT clay at 8.6% ash loading reduced impact strength by 90%; M₂(HT)₂-125 clay at 7.9% ash loading reduced impact strength by 85%. This is to be expected given that we were adding inorganic filler to the ABS.

The third investigation dealt with the comparison of incorporating (HE)₂MT clay at about 3% ash loading into a high rubber content ABS system *via* two different processing methods, simultaneous and masterbatch, in order to investigate how the processing sequence affects the fire retardancy for ABS/MMT clay blends. The results reveal that differences in processing method did not result in noticeably different fire retardant behavior, since the PHRR curves of simultaneous-extruded ABS/(HE)₂MT blends were almost congruent with the PHRR curves of masterbatch-extruded blends. No noticeable differences in modulus were observed at small clay loading between the two processing methods. Also, impact strength dropped significantly for either processing method.

In conclusion, SAN/clay is a good model for the effects of extrusion on clay morphology in the more complex ABS/clay blends. In both matrices, modulus was enhanced, tensile strength fell, and toughness fell. The drop in tensile strength was mitigated by rubber content. Fire retardant behavior, as measured by PHRR, was

improved at high clay loadings for both SAN and ABS blends. All blends tested resulted in either a mixed intercalated/exfoliated clay morphology or an unintercalated morphology, as confirmed by XRD. Processing sequence in the ABS/clay blends did not affect properties significantly, either mechanical or fire retardant.

REFERENCES

- 1 Pescovtz, D., "Please Dispose of Properly," *Scientific American*, **282**, #2, 33, February, (2000).
- 2 Gachter, R., Muller, H., Plastics Additives Handbook, 4th ed; New York, 715-721, (1996).
- 3 Sjodin, A., Hagmar, L., Klasson-Wehler, E., Kronholm-Diab, K., Jakobsson, E., Bergman, A., "Flame Retardant Exposure: Polybrominateddiphenyl Ethers in Blood from Swedish Work," *Environmental Health Perspectives*, **107**, #8, 643-648, August, (1999).
- 4 Pinnavai, T. J., Beall, G. W., eds; Polymer-Clay Nanocomposites, Wiley & Sons, New York, 195-204, (2000),
- 5 Yano, K., Usuki, A., Okada, A., Kurauchi, T., "Synthesis a Properties of Polyimide-clay Hybrid," *J. Polym. Sci.*, **31**, 2493-2498, (1993).
- 6 Gilman, J. W., "Flammability and thermal stability studies of polymer layered-silicate (clay) nanocomposites," *Appl. Clay Sci.*, **15**, 31-49, (1999).
- 7 Kroschurtz, J. S., Kirk-Othmer Encyclopedia of Chemical Technology, 4th ed; John Wiley & Sons, New York, **1**, 391, (1993).
- 8 Paul, D. R., Barlow, J. W., Keskkula, H., Encyclopedia of Polymer Science & Engineering, 2nd ed; Wiley, New York, **2**, 339-461, (1988).
- 9 Kroschurtz, J. S., Kirk-Othmer Encyclopedia of Chemical Technology, 4th ed; John Wiley & Sons, New York, **1**, 399, (1993).
- 10 Communications with Wadhera, I., Senior Engineer of IBM, November, (2000).

- 11 Ralph, E., Clay Mineralogy, 2nd ed; McGraw-Hill Book Company, New York, 78-79, (1968).
- 12 Blumstein, A., *Bull. Chim. Soc.*, 899, (1961).
- 13 Usuki, A., Kojima, Y. Kawasumi, M., "Synthesis of Nylon 6-clay Hybrid," *J. Mater. Res.*, **8**, 1179-1184, (1993).
- 14 Kojiman, Y., Usuki, A., Kawasumi, M., "Mechanical Properties of Nylon 6-clay Hybrid," *J. Mater. Res.*, **8**, 1185-1189, (1993).
- 15 Lan, T., Pinnavaia, T. J., "Clay-Reinforced Epoxy Nanocomposites," *Chem. Mater.*, **6**, 2216-2219, (1994).
- 16 Jeon, H. G., Jung, H. T., Lee, S. D., Hudson, S., *Polym. Bull.*, **41**, 107, (1998).
- 17 Giannelis, E., *Advd. Mater.*, **8**, 29, (1996).
- 18 Fisher, H., Gielgens, L., Koster, T., "Nanocomposites from Polymers and Layerer Minerals," TNO-TPD report, (1998).
- 19 Fujiwara, S., Sakamoto, T., "Method for Manufacturing a Clay-Polyamide Composite," Kokai Patent Application, no. SHO 51(1976)-109998.
- 20 Burnside, S. D, Giannelis, E. P, *Chem. Mater.*, **7**, 1587, (1995).
- 21 Lee, J., Giannelis, E., *Polymer Preprints*, **38**,688-689, (1997).
- 22 Gilman, J., Kashiwagi, T., Lichtenhan, J., *SAMPE Journal*, **33**, 40-46, (1997).
- 23 Gilman, J., Kashiwagi, T., Lomakin, S., Giannelis, E., "Fire Retardancy of Polymers: the Use of Intumescence," The Royal Society of Chemistry, Cambridge, (1998).
- 24 Babrauskas, V., Peacock, R. D., *Fire Safety Journal*, **18**, 255, (1992).
- 25 Richard E. L., *Fire Matl*, 179-186, (2000).

- 26 Fornes, T. D., Yoon, P. J., Keskkula, H, Paul, D. R., “ Nylon 6 Nanocomposites: The Effect of Matrix Molecular Weight”, *Polymer*, **42**, 9929, (2001).
- 27 Krishnamoorti, R., Yurekli, K., “Rheology of Polymer Layered Silicate Nanocomposites”, *Current Opinion in Colloid & Interface Science*, 6, 464-470, (2001).
- 28 Stretz, H. A., Koo, J. H., Dimas, V. M., Zhang, Y., “Flame Retardant Properties of Polycarbonate/Montmorillonite Clay Nanocomposites Blends”, *Polymer Preprints*, **42**, 50, (2001).